Determination of non-Markovinity in the Jaynes-Cummings Model

Determinación de la no-Markovianidad en el Modelo de Jaynes-Cummings

Presented by MANUEL ALEJANDRO RAMOS ARIAS

A Thesis submitted in fulfillment of requirements for the degree of
Bachelor of Science in Physics

Facultad Ciencias Naturales y Exactas
Departamento de Física - 3146
Sede Cali, Valle del Cauca

Advisor:
Dr.rer.Nat. Arturo Argüelles Parra

Co-Advisor
Dr. Carlos Augusto Galíndez Jamioy

September, 2024
Cali, Valle del Cauca, Colombia

ABSTRACT

In this work, we outline an innovative proposal on the basis of a powerful data analysis technique, known as principal component analysis (abbreviated PCA), to characterize and quantify the degree of non-Markovianity of an open quantum physical system. In particular, the method to be introduced is applied to the Jaynes-Cummings model, whose dynamical behavior is geometrically illustrated by the Bloch sphere representation. Finally, our proposal is compared in a qualitative way with other proposals frequently used in the literature to demonstrate the great advantage it offers as a suitable non-Markovianity quantifier, both because of the enormous computational advantage it brings with, as well as because it takes into account a wider range of accessible quantum states that contribute to the construction of a more complete and general measure.

Key Words: Non-Markovianity, Information Backflow, Principal Component Analysis.

RESUMEN

En este trabajo se esboza una innovadora propuesta basada en una potente técnica de análisis de datos, conocida como análisis de componentes principales (abreviado PCA por sus siglas en inglés), para caracterizar y cuantificar el grado de no Markovianidad de un sistema cuántico abierto. En particular, el método que se va a introducir se aplica al modelo de Jaynes-Cummings, cuyo comportamiento dinámico se ilustra geométricamente mediante la representación en la esfera de Bloch. Finalmente, nuestra propuesta se compara de forma cualitativa con otras propuestas frecuentemente utilizadas en la literatura para mostrar la gran ventaja que ofrece como un cuantificador de no Markovianidad adecuado, tanto por la enorme ventaja computacional que trae consigo, como porque tiene en cuenta un rango más amplio de estados cuánticos accesibles que contribuyen a la construcción de una medida más completa y general.

Palabras Clave (en inglés): Non-Markovianity, Information Backflow, Principal Component Analysis.

ACKNOWLEDGMENTS - AGRADECIMIENTOS

En primera instancia, agradezco al pilar fundamental de mi existencia: mis padres. Quiero agradecer a mi mamá por ser esa persona que me dio la vida, por sus innumerables enseñanzas y consejos, por acompañarme y por siempre estar a mi lado, por ser esa luz guía en mis momentos de incertidumbre, por creer siempre en mí y por ser una de mis mayores motivaciones. Simplemente gracias, mamá, por ser la persona más importante en mi vida. Quiero darle las gracias y dedicarle este Trabajo de Grado a mi papá, a ese ser que partió hace poco más de un año y cuya ausencia aún duele profundamente. Aunque estas son de las primeras palabras que aparecen en este documento, la realidad es que fueron las últimas que fui capaz de plasmar. A pesar de la gran cantidad de intentos, de lágrimas y de horas dedicadas para expresar la inmensa gratitud y el amor que le guardo a mi señor padre, la verdad es que no existen palabras que puedan sintetizar o encapsular todas las emociones y pensamientos que vienen a mi mente al evocar su figura. Por más que ya no estés físicamente con nosotros, tu huella siempre vivirá y se mantendrá presente en lo profundo de mi ser y de mi alma. Siempre te amaré papá. Gracias por todo.

Quiero dar las gracias a ese otro pilar fundamental de existencia: mi hermosa Familia. Quiero agradecer a todos mis familiares con los que he tenido la oportunidad y el privilegio de interactuar, por todas esos valores y enseñanzas que han inculcado en mí y, en especial, por todo ese cariño y amor que he recibido. Ustedes han sido el motor de mi vida. Me siento muy orgulloso y privilegiado de contar (o a haber contado) con tan bellas personas en el transcurso de mi historia.

Quiero dar las gracias a nuestra Universidad del Valle, por ser esa institución que me brindó la oportunidad y las herramientas para formarme como profesional. Gracias al cuerpo docente de la Facultad de Ciencias Naturales y Exactas, y en particular a los profesores e investigadores del Departamento de Física, por sus aportes directos a mi formación académica durante mi proceso educativo en la Universidad. Gracias a los profesores y a mis compañeros del Grupo de Óptica Cuántica, el grupo de investigación al que pertenecí, por guiarme en estos primeros contactos con la investigación científica. Gracias a los Funcionarios de la Universidad, pues sin su valioso aporte, la Universidad del Valle sería un espacio muy diferente al que disfruté en estos últimos años.

Quiero hacer ahora una mención especial y brindarle el reconocimiento que se merecen todas esas amistades que he conformado en el transcurso de los años, tanto dentro como fuera del ámbito académico. Considero que estas personas constituyen un componente sustancial dentro de mi desarrollo personal y social, así como una parte indispensable de mi vida. Mi intención en este momento no es entrar en particularidades, porque, afortunadamente para mí, la lista sería interminable. Sin embargo, si estas líneas arriban a ustedes en algún momento, quiero expresar en ellas mis más profundos y sinceros agradecimientos, por su amistad incondicional y por todo el apoyo que me han ofrecido en los procesos que he afrontado durante mi diario vivir. Espero que yo también haya podido dejar una huella tan profunda y hermosa en sus vidas, como las que ustedes han dejado en mí.

Contents

CHAPTER 1

Introduction

The theoretical study and technological implementation of quantum theory have occupied a central spotlight in the development of scientific research over the last decades and in the advancement of contemporary society. It is a natural presumption that one of the fundamental requirements for the realization of quantum technologies must be the preservation of quantum characteristics of physical systems. This is guaranteed for isolated quantum systems, for which the time evolution of the state containing all the relevant information about the system is governed by the Schrödinger equation according to the postulates of quantum mechanics [1].

Although the above approach is successful in certain cases, the reality is that the isolation of physical systems is no more than an idealization as the interaction of the system of interest with its environment is inevitable, carrying with it constant exchanges of energy and information between the two. Such interactions lead to the phenomenon of quantum decoherence and, as a consequence, the emergence of a purely classical behaviour of the formerly quantum system [2]. It then becomes necessary to provide a proper formalism to deal with these more complex issues and this is the reason for the rise of the theory of open quantum systems [3, 4].

In this framework, it is a common practice to study the temporal evolution of the system coupled to the environment as a whole, rather than each of them individually. Then, information concerning only the system of our interest can be extracted by tracing over all the degrees of freedom of the environment. Despite the generality of this procedure, the associated mathematical treatment and the solutions found (if any) are typically quite complex and daunting to deal with. This is why over the years various approximations have been proposed to simplify the calculations, being undoubtedly the Born-Markov approximation the most famous and the most used one.

Systems for which this approximation is valid are the so-called Markovian systems, and in order for it to be properly applicable, certain physical considerations must be required [5], such as a weak system-environment coupling, short environment correlation time or large size of the environment compared to that of the system. These lead to the solution of a master equation in the Lindblad form [6, 7] and local in time, the latter meaning that the states of the system at subsequent times depend exclusively on the state of the system at the present time. In this regard, the term *memoryless* is coined to refer to Markovian systems because their dynamics is not influenced by their past history.

Recently, however, with the technological advances developed particularly in the area of quantum control [8–15], the Born-Markov approximation has become inadequated and insufficient for the description of substantial portion of open quantum systems. It has thereby proved necessary to develop a formalism and

strategies to deal with systems that go beyond the already mentioned approximation, thus giving birth to the research field of non-Markovianity. Within this regime, we can observe the phenomena of recoherence and backflow information from the environment to the system [16, 17], and, consequently, the most characteristic feature of this class of systems: the memory effects.

The study of non-Markovian systems has shown the advantage they provide for quantum information tasks and applications such as quantum evolution speedup [18], quantum control processes [19], teleportation protocols using mixed states [20], entangled states preparation [21, 22], quantum metrology [23] and efficient extraction of work in the Otto cycle [24], just to mention a few. These implementations show the potential of non-Markovian systems of being a fundamental factor in the development of future technologies.

Then, having the ability to identify whether the dynamics of an open quantum system presents a Markovian or non-Markovian behavior becomes a relevant task to be considered. Nevertheless, there is a wide variety of proposals to define either a quantifier for the degree of non-Markovianity of a system, or simply to serve as witnesses of the presence of non-Markovian characteristics, being the most widely used the proposals of Breuer-Laine-Piilo (BLP measure) [16] and of Rivas-Huelga-Plenio (RHP measure) [25]. The main problem lies in the fact that the different proposals are defined on the basis of different criteria and, consequently, different results are obtained depending on the chosen quantifier. In this aspect it has not been possible to establish a consensus on how to determine the degree of non-Markovianity of an open quantum system, so this is still an ongoing issue for debate and research.

In this work, we outline an innovative proposal on the basis of a powerful data analysis technique, known as principal component analysis (abbreviated PCA), to characterize and quantify the degree of non-Markovianity of a physical system. In particular, the method to be introduced is applied to the Jaynes-Cummings model, whose dynamical behavior is geometrically illustrated by the Bloch sphere representation. Finally, our proposal is compared with other proposals frequently used in the literature to demonstrate the great advantage it offers as a suitable non-Markovianity quantifier.

The work is structured as follows. In Chapter 2 a brief introduction to the theory of open quantum systems will be given, making special mention of the conceptual and technological importance of non-Markovian systems, to finally present some widely used non-Markovian quantifiers. In Chapter 3 we will present the Jaynes-Cummigns model on which the proposed techniques will be applied later, and special emphasis will be given to the representation of quantum states on the Bloch sphere. In Chapter 4 a formal presentation of the proposed methodology for characterizing and quantifying non-Markovianity will be made, with a subsequent discussion comparing qualitatively our proposal with others. In Chapter 5 some conclusions of the work and future perspectives will be outlined.

CHAPTER 2

Quntifiers of non-Markovianity

2.1 THEORY OF OPEN QUANTUM SYSTEMS

From the postulates of quantum mechanics [1], all the information regarding a physical system is contained in a vector state (also commonly known as ket) denoted by $|\psi\rangle$ and belonging to a complex Hilbert space, from which all its relevant properties can be extracted. Its temporal evolution can be determined by means of the Schrödinger equation

$$i\hbar\frac{d}{dt}\,|\psi(t)\rangle = H(t)\,|\psi(t)\rangle\,, \tag{2.1}$$

being $i=\sqrt{-1}$ the imaginary unit, $\hbar$ the reduced Planck constant having units of action (energy multiplied by time) and H the Hamiltonian operator associated with the physical system.

The solution of the above differential equation involves an unitary evolution operator $U(t,t_0)$, whose exact form relies on the dependence of the Hamiltonian with time

$$U(t,t_0) = T_{\leftarrow}\exp\left[-i\int_{t_0}^{t} ds H(s)\right], \tag{2.2}$$

where $T_{\leftarrow}$ denotes the time-ordering operator, with the task of reordering the product of the time-dependent operators in chronological order as indicated by the arrow, i.e. such that their time arguments increase from right to left. In particular, for time-independent Hamiltonians, the evolution operator is simply expressed as $U(t,t_0)=\exp\left[-iH(t-t_0)\right]$.

Besides that, the unitary operator must satisfy $U(t,t_0)U^{\dagger}(t,t_0) = 1 = U^{\dagger}(t,t_0)U(t,t_0)$ and is used to determine the state of the system at an arbitrary time t starting from some known initial state defined at a fixed time t_0

$$|\psi(t)\rangle = U(t,t_0)|\psi(t_0)\rangle\,. \tag{2.3}$$

On the other hand, to be more formal, it has to be mentioned that the ket $|\psi\rangle$ is only suitable to represent the so-called pure states. However, we do not always have access to all the complete information about a physical system, but only a fraction of it due to lack of knowledge. It is here where the representation by means of the density matrix ρ becomes relevant as it is a mathematical element of greater generality, since it allows us to represent the aforementioned pure states, but also the so-called mixed states. The density matrix is defined as

$$\rho(t) = \sum_{\alpha} w_\alpha(t)\,|\psi_\alpha(t)\rangle\langle\psi_\alpha(t)|\,, \tag{2.4}$$

where $0\leq w_\alpha\leq 1$ is the probability that the system is described by the pure state $|\psi_\alpha\rangle$. We do not know with certainty what pure state the system is in, but we have a range of options, each with its respective

probability. Of course, it should be required that $\sum_\alpha w_\alpha(t) = 1$ in every instant of time. For completeness, we mention that the density matrix associated with a pure state $|\phi\rangle$ has the simple form $\rho = |\phi\rangle\langle\phi|$.

The time evolution of the density matrix is expressed by the von Neumann equation (also known as Liouville-von Neumann equation because of its similarity to the Lioville equation of classical mechanics [26])

$$\frac{d}{dt}\,\rho(t) = -\frac{i}{\hbar}\,[\,H(t), \rho(t)\,]\,, \tag{2.5}$$

where [,] denotes the commutator between two operators in quantum mechanics, which is defined as $[A, B] = AB - BA$. Furthermore, the solution for the von Neumann equation is given again in terms of the unitary time evolution operator

$$\rho(t) = U(t, t_0)\;\rho(t_0)\;U^\dagger(t, t_0)\;. \tag{2.6}$$

The mathematical formalism just presented is ideal for the dynamical study of isolated quantum systems. Nonetheless, when the interaction (or to be more concise, the coupling) between the system of interest and its environment (which is also a quantum system) becomes so relevant that it can no longer be ignored, the method of unitary time evolutions becomes obsolete. This resides in the fact that the coupling between both physical systems builds correlations between them [4], so that the description of the problem in terms of the individual systems separately, described by unitary evolutions, is incomplete. It then becomes necessary to consider another mathematical formalism that encompasses the treatment of the so-termed open quantum systems.

A first strategy one might think of, to solve this dilemma, is to consider a larger physical system constituted by the system of interest (henceforth denoted as S) and by its environment (denoted E) [27]. The fundamental idea behind this is that the system composed of the now called subsystems S and E, is a closed quantum system on which the tools of time evolution by means of unitary operators can be applied.

The associated Hamiltonian is usually divided into the Hamiltonians of the systems S and E separately (H_S and H_E respectively), plus an interaction Hamiltonian (H_{SE}) describing the coupling between them

$$H = \underbrace{H_S + H_E}_{H_0} + H_{SE}\;. \tag{2.7}$$

It is typical to think of H_{SE} as a composition of cross products between the operators belonging to the Hilbert spaces of the subsystems.

For the construction of the density matrix of the composed system, here denoted by χ, it is common to assume that at the initial instant t_0, set here as $t_0 = 0$ for the sake of simplicity, there are still no correlations between the system of interest and its environment, i.e. their interaction has not yet taken place, so that the density matrix χ at that initial instant can be constructed as a direct tensor product of the initial density matrices of S and E

$$\chi(0) = \rho_S(0) \otimes \rho_E(0)\;. \tag{2.8}$$

Thus, following equation 2.6, the time evolution of the density matrix for the composed system is described as

$$\chi(t) = U(t, 0)\,[\,\rho_S(0) \otimes \rho_E(0)\,]\,U^\dagger(t, 0)\;. \tag{2.9}$$

Nevertheless, we face a problem at this stage since the information concerning the environment E, which is contained in χ, is only of indirect interest for our purposes and a detailed description of it is not necessary. In order to recover the information concerning only our system of interest S, we use the partial trace over all the degrees of freedom of the environment, thus obtaining the so-called reduced density matrix of the subsystem

$$\rho_S(t) = Tr_E\,\{U(t, 0)\,[\,\rho_S(0) \otimes \rho_E(0)\,]\,U^\dagger(t, 0)\}\;. \tag{2.10}$$

In spite of the fact that the solution presented in equation 2.10 is the most general possible for the treatment of open quantum systems, the mathematical expressions obtained from it are usually extremely cumbersome and difficult to deal with. For this reason, some approximations have been considered in order to lighten the calculations and to reveal the physics that is sometimes lost in the complexity of the associated mathematics. The most widespread and extensively used one is the called Markov approximation, or to be more concise the Born-Markov approximation, grounded on physical assumptions such as [5] a weak system-environment coupling, a short environment correlation time or a large size of the environment compared to that of the system.

Therefore, considering in particular a large environment ("large" in the sense of number of degrees of freedom compared to those of the subsystem S) and a weak system-environment coupling, it is to be expected that E is not considerably affected by its coupling with S, so that its quantum state ρ_E can be assumed constant in time. On the other hand, S is expected to change appreciably as it is a physical system much smaller than its environment E, so its time dependence remains important in the study of the problem. In this way, the density matrix of the composed system for each time can be written as

$$\chi(t) = \rho_S(t) \otimes \rho_E \ . \tag{2.11}$$

This change has strong implications from a physical point of view, as will be seen further on. From the mathematical point of view it also has interesting immediate implications, since it allows us to define a map $V(t)$ from the space $\mathcal{S}(H_S)$ of density matrices of the reduced system into itself [3]

$$\rho_S(t) = V(t)\rho_S(0) \ , \tag{2.12}$$

where

$$V(t) : \mathcal{S}(H_S) \to \mathcal{S}(H_S) \tag{2.13}$$

is called a dynamical map, which can be fully characterized in term of operators belonging to the Hilbert space $\mathcal{S}(H_S)$.

This dynamical map has to be a completely positive and trace-preserving quantum operation [28]. Recall that a quantum mapping is positive (also positive-semidefinite) if the eigenvalues of the resulting operator are non-negative. This is indispensable in the present context when applying the mapping on density matrices, so that they can represent valid physical states. Now the stronger condition of being completely positive is necessary when applying the mapping to a single part of a composed system, again resulting in a positive operator. Mathematically this implies that $(V(t) \otimes \mathbb{I}_E) \geq 0$, being $\mathbb{I}_E$ the identity operator related to the environment. On the other hand, the trace-preserving feature is necessary to fulfill the basic properties of the density matrices after applying the mapping.

In addition, the dynamical map obeys the semigroup property, defined as

$$V(t_1)V(t_2) = V(t_1 + t_2), \quad t_1, t_2 \geq 0 \ . \tag{2.14}$$

This is very interesting and it is noteworthy that this same property is fulfilled by Markovian processes in the purely classical formulation, which is usually expressed by the Chapman-Kolmogorov differential equation [29].

Under certain mathematical conditions [6, 7], a quantum dynamical semigroup map $V(t)$ can be expressed in exponential form by means of the generator $\mathcal{L}$ of the semigroup as follows

$$V(t) = \exp\left(\mathcal{L}t\right) \ . \tag{2.15}$$

By introducing this expression in equation 2.12 and then taking the time derivative, it is obtained that

$$\frac{d}{dt}\rho_S(t) = \mathcal{L}\ \rho_S(t) \ , \tag{2.16}$$

known as the Markovian quantum master equation.

The most important feature of the above expression is that it is local in time, as both sides of the differential equation are evaluated at the same time instant. This implies that the future evolution of the reduced density matrix (the states of the system at subsequent times) depends exclusively on its state at the current instant of time, since it does not make any reference at all to states during previous times, i.e. it does not take into account its past history. In this sense, Markovian systems are said to be memoryless.

The effect of the semigroup generator $\mathcal{L}$ on the reduced density matrix (right-hand side of equation 2.16) is usually written in the so-called Lindblad form

$$\mathcal{L}\,\rho_S = -i\,[H, \rho_S] + \sum_k \gamma_k \left(L_k \rho_S L_k^\dagger - \frac{1}{2} L_k^\dagger L_k \rho_S - \frac{1}{2} \rho_S L_k^\dagger L_k \right) , \tag{2.17}$$

where the first term refers to the unitary evolution given by the von Neumman equation, L_k are the so-called Lindblad operators, and γ_k are dimensionless parameters that are determined from the system-environment correlation functions and play the role of relaxation rates. These parameters and operators can be made explicit by making use of some methods [30–33]. We should also note that usually the part associated with the summation is called the dissipator and $\mathcal{L}$ is usually named as a super-operator, since it acts on other operators and its effect results in operators.

To conclude this section regarding the quantum Markovian study, it is worth mentioning that apart from the master equation method just presented, there also exist other methods of analysis widely employed in the field of study of open quantum systems, such as [34] phase-space representations, Fokker-Planck equations and stochastic differential equation, among others.

2.2 BEYOND THE MARKOV APPROXIMATION

The ”memoryless” concept that characterizes the Markovian dynamics can be interpreted as a unilateral transfer of information from the system to the environment, with no returns to the system at any time [4]. This implies that the information initially contained in the quantum system of interest is gradually erased as time passes. Here relies one of the major problems encountered in the correct implementation of technologies based on quantum mechanics, since it is natural to think that one of the main prerequisites for its realization must be the conservation of the quantum properties of physical systems in the times in which the experiments are carried out.

From the formalism of Markovian systems, it seems an impossible task to accomplish. In recent years, however, technological developments have made it possible to study and work with quantum systems for which the Born-Markov approximation is not applicable [8–15], thus giving birth to the research field of non-Markovianity. The non-Markovian systems exhibits, for example, the phenomena of recoherence and backflow information from the environment to the system [16, 17], and, consequently, the most characteristic feature of this class of systems: the memory effects.

The study of non-Markovian systems has shown the advantage they provide for quantum information tasks and applications such as quantum evolution speedup [18], quantum control processes [19], teleportation protocols using mixed states [20], entangled states preparation [21, 22], quantum metrology [23] and efficient extraction of work in the Otto cycle [24], just to mention a few. These implementations show the potential of non-Markovian systems of being a fundamental factor in the development of future technologies.

On the other hand, having the ability to identify whether the dynamics of an open quantum system presents a Markovian or non-Markovian behavior becomes a relevant task to be taken into account for

the study of the system itself and for the possible applications linked to it. In this direction, different non-Markovian quantifiers have been proposed in the literature to determine, on one side, the nature of the quantum systems coupled to their environment, and, on the other, to be able to compare systems that fit within the non-Markovian description of the problem and determine for example which one has more marked non-Markovian properties than the other.

Nevertheless, there is a wide variety of proposals to define either a quantifier for the degree of non-Markovianity of a system, or simply to serve as witnesses of the presence of non-Markovian characteristics. The main problem lies in the fact that the different proposals are defined on the basis of different criteria and, consequently, different results are obtained depending on the chosen quantifier. In this aspect it has not been possible to establish a consensus on how to determine the degree of non-Markovianity of an open quantum system, so this is still an ongoing issue for debate and research. Precisely the objective of the present work arises in this line and is focused on presenting a novel proposal to quantify the non-Markovianity in an suitable way. However, this will be the subject of discussion in Chapter 4.

Let us recall that the time evolution of the reduced density matrix of the sistem of interest can be described by means of a family of dynamical maps, here denoted by Φ_t, which must be completely positive and trace-preserving (CPTP). It is usual to call these quantum operations also as quantum channels [28]. The dynamical map is said to be divisible when it can be written as the composition of two CPTP maps

$$\Phi_t = \Phi_{t,\tau}\,\Phi_{\tau,0}\,, \qquad \forall\,\tau \leq t\,. \tag{2.18}$$

Nondivisibility occurs therefore if there exits times τ for which $\Phi_{t,\tau}$ is not CPTP. It is a common feature of all non-Markovianity measures to be grounded on the non-monotonic behavior with respect to time of certain quantities when the divisivity property is broken. In contrast, the opposite is not necessarily true: i.e. the non-monotonic behavior of the quantities to be chosen does not imply non-divisibility of the dynamical map. In the following, a substantial portion of the quantifiers will be presented, with particular emphasis on the two most widely used: the Rivas-Huelga-Plenio (RHP) and the Breuer-Laine-Piilo (BLP) proposals.

2.2.1 The Rivas-Hulga-Plenio (RHP) Measure

The proposal presented by RHP [25] aims to quantify non-Markovianity from the departure of the intermediate map $\Phi_{t,\tau}$ from that which would be CPTP. Being mathematically more formal, the dynamical maps Φ_t can be represented by Kraus operators [35] or by Choi-Jamiołkowski matrices [36, 37]. Under the second representation, the Choi-Jamiołkowski matrix $C(\Phi_t)$ is positive (also positive-semidefinite) if and only if Φ_t is a quantum channel, or in other words a CPTP map. Therefore, the negativity of the Choi-Jamiołkowski matrix can be used as a non-Markovianity measure.

In this way, the RHP quantifier $\mathcal{N}_{RHP}$ is defined as

$$\mathcal{N}_{RHP}(\Phi_t) = \int_0^\infty g(t)dt\,, \tag{2.19}$$

where

$$g(t) \equiv \lim_{\epsilon\,\to\,0^+} \frac{\mathrm{Tr}\mid C(\Phi_{t+\epsilon,t})\mid -1}{\epsilon}\,, \tag{2.20}$$

in which ϵ is a parameter encompassing the time course and the trace norm $\mathrm{Tr}|\cdot|$ is defined as

$$\mathrm{Tr}|A| = \mathrm{Tr}\sqrt{AA^\dagger}\,, \tag{2.21}$$

being equal to the sum of the singular values of the matrix A, which are defined as the roots of the eigenvalues of $AA^\dagger$ [38]. Note that the singular values are non-negative too.

For CPTP maps, the auxiliar function $g(t)$ takes the value of zero. Therefore, if for every instant of time the divisibility condition is satisfied, then $\mathcal{N}_{RHP} = 0$, indicating that the system follows a Markovian dynamics (memoryless). In contrast, a non-Markovian signature is obtained when $\mathcal{N}_{RHP} \neq 0$, where it should be made clear that the higher the value of $\mathcal{N}_{RHP}$, the more non-Markovian the system is.

2.2.2 The Breuer-Laine-Piilo (BLP) Measure

The proposal presented by BLP [16] is arguably the most famous and widely used non-Markovianity quantifier in the literature. The measure is based on the violation of the non-monoticity of the distinguishability between quantum states, which can be interpreted as an information backflow from the environment to the system. The distinguishability can be viewed as a way to quantify the ammount of information contained in a quantum system since the more we know about the system, the more information we have about it, and finally the more we are able to distinguish between quantum states.

Here the distinguishability between the quantum states ρ_1 and ρ_2 is characterized by the trace distance $\mathcal{D}$, defined as half of the trace norm

$$\mathcal{D}(\rho_1, \rho_2) = \frac{1}{2} \text{Tr} \sqrt{(\rho_1 - \rho_2)\,(\rho_1 - \rho_2)^\dagger}\,, \tag{2.22}$$

which takes real values from 0 to 1. It is noteworthly that if the quantum states are orthogonal (completely distinguishable), then $\mathcal{D}(\rho_1, \rho_2) = 1$. If, on the other hand, they represent the same quantum state, it is clear that $\mathcal{D}(\rho_1, \rho_2) = 0$.

Under CPTP maps, the trace distance is contractive, meaning that the distinguishability between the two initial states ${\rho_0}^1$ and ${\rho_0}^2$ decreaces in a continuous and monotonic manner over time. Mathematically, when the divisibility property is satisfied, the time derivative of the trace distance (denoted by σ) is always negative or equal to zero

$$\sigma\,({\rho_0}^{1,2}, t) = \frac{d}{dt}\,\mathcal{D}({\rho_t}^1, {\rho_t}^2) \leq 0 \qquad \text{(under CPTP maps)}\,. \tag{2.23}$$

The quantity σ is interpreted in the work of BLP as an information flux from the system to the environment. Its negative values then indicate an irreversible loss of the information initially contained in the system of interest due to the coupling. This is a characteristic feature of a Markovian behavior.

In this order of ideas, positive values of σ would suggest a backflow information to the system, which is typified by a non-monotonicity of the trace distance. Consequently, the non-Markovianity measure $\mathcal{N}_{BPL}$ is constructed by summing over all periods of non-monoticity of the information flux, with the additional task of optimizing over all pairs of initial states of the system

$$\mathcal{N}_{BPL} = \max_{{\rho_0}^{1,2}} \int_{\sigma>0} \sigma({\rho_0}^{1,2}, t)\, dt\,. \tag{2.24}$$

The optimization problem is extremely laborious from the computationally point of view, and is specially demanding when dealing with non low-dimension multipartite systems [39]. Although it has been shown that the optimal pair of initial conditions that maximize $\mathcal{N}_{BLP}$ must belong to the boundary of the space state of the system and must be orthogonal to each other [40], the optimization is still one of the major drawbacks of this method, but is not the only. However, a more extensive discussion will be postponed until Chapter 4, when it will be directly compared with our method not yet presented.

On the other hand, it should be mentioned that the non-Markovian processes characterized by the BLP measure are always nondivisible; notwithstanding the converse implication is not necessarily true [41]. This is partly where the discrepancy between the different non-Markovianity quantifiers lies, since if one takes the divisivity condition as a foundation, then the backflow information must be viewed only as a witness, but not as an irrefutable proof of non-Markovian behavior. Nonetheless, this is only a matter of defining the criteria, and the opposite situation could also be contemplated.

2.2.3 Others non-Markovianity measures and witnesses

There are many proposals that follow the idea suggested by BLP, i.e. they are based on the violation of the monoticity of some distance when the dynamical map is nondivisible. Within this category are the Bures distance [42] and the Bures angle [43] (both based on fidelity, which in itself is not a metric), the statistical distance [44], the relative entropy [45], the Bhattacharyya distance [46], and so on [47].

Other nonmonotonic quantities that can be used as a measure or witness of non-Markovianity include the quantum mutual information [48], focused on the study of the system-environment correlations; the flow of quantum Fisher information [49], which also characterizes the statistical distinguishability of the reduced density matrix; Hall-Creser-Li-Anderson (HCLA) measure [50], which relies on negative decays rates of the master equation; local quantum uncertainty [51], the accesible information [52], and the volume in the space state representation [53], just to mention a few. Even machine learning techniques have been applied to determine the degree of non-Markovianity of quantum systems [54, 55].

CHAPTER 3

Jaynes-Cummings Model

The Jaynes-Cummings model [56] (abbreviated JCM) is the simplest way to describe the interaction between light and matter when both are considered as quantized, that is under the formalism of second quantization. Within its assumptions, the matter is modeled as a two-level atomic system and the light as a single quantized mode of a bosonic field. Despite its apparent simplicity, this model has been used for several years in diverse areas of scientific research, among which are atomic physics, quantum optics, solid-state physics and quantum information [57–59]. In the context of non-Markovian dynamics, the main subject of study of this work, the JCM represents a good example of a system exhibiting this type of behavior due to its characteristic phenomenon of revivals of atomic populations, which can be interpreted as a memory effect and will be discussed later in this chapter.

3.1 MATHEMATICAL FORMULATION

The formulation of the JCM is strongly influeced by a predecessor model in the description of light-matter interaction and of semiclassical character, meaning that matter is treated under the laws of quantum mechanics, while the radiation field is treated under classical electrodynamics. This is the Rabi model [60], developed in the context of research on nuclear magnetic resonance. Moreover, the JCM is sometimes referred to as the fully quantum mechanical Rabi model.

From now on, unless otherwise stated, the Planck system of natural units [61] will be used as standard. This shortens the writing of equations by defining, among others, $\hbar = 1$ and $c = 1$.

Our starting point will be the classical Hamiltonian describing an electron of mass m and charge e bounded to an atomic nucleus in the presence of an external electromagnetic field, given by [62]

$$H(\mathbf{r},t) = \frac{1}{2m}\left[\mathbf{p} + e\mathbf{A}(\mathbf{r},t)\right]^2 - e\,\Phi(\mathbf{r},t) + V(r), \tag{3.1}$$

where $\mathbf{p}$ is the momentum operator associated with the electron, $\mathbf{A}$ is the vector potential and Φ the scalar potential representing the external classical field, and V is the Coulomb interaction binding the electron to the nucleus.

From classical electrodynamics, it is well-known that the representation of the external electromagnetic field through the vector and scalar potentials $\mathbf{A}$ and Φ is invariant under gauge transformations [63]

$$\mathbf{A}'(\mathbf{r},t) = \mathbf{A}(\mathbf{r},t) + \nabla\lambda(\mathbf{r},t), \tag{3.2}$$

$$\Phi'(\mathbf{r},t) = \Phi(\mathbf{r},t) - \frac{\partial\lambda(\mathbf{r},t)}{\partial t}, \tag{3.3}$$

where $\lambda(\mathbf{r},t)$ is an arbitrary scalar function.

In the present framework, it is desirable to choose the Coulomb gauge, also known as radiation gauge, which satisfies $\Phi = 0$ and the transversality condition $\nabla \cdot \mathbf{A} = 0$. Its main feature is that it allows to represent the external field only by means of the vector potential $\mathbf{A}$, but it has the drawback of not being relativistic invariant. However, this drawback does not generate significant problems in the work area of quantum optics, where non-relativistic formalism is adequate [64]. Thus, the gauge transformed Hamiltonian becomens

$$H'(\mathbf{r},t) = \frac{1}{2m}\{\ \mathbf{p} + e\left[\mathbf{A}(\mathbf{r},t) + \nabla\lambda(\mathbf{r},t)\right]\ \}^2 + e\frac{\partial\lambda(\mathbf{r},t)}{\partial t} + V(r). \tag{3.4}$$

Finally, we choose the gauge function $\lambda(\mathbf{r},t) \equiv -\ \mathbf{r}\cdot\mathbf{A}(\mathbf{r},t)$, so that the resulting transformed Hamiltonian is

$$H'(\mathbf{r},t) = \frac{\mathbf{p}^2}{2m} + V(r) + e\ \mathbf{r}\cdot\frac{\partial\mathbf{A}(\mathbf{r},t)}{\partial t}\ . \tag{3.5}$$

Besides that, for no sources near the atom, the vector potential $\mathbf{A}$ satisfies the wave equation

$$\nabla^2\mathbf{A}(\mathbf{r},t) - \frac{\partial^2\mathbf{A}(\mathbf{r},t)}{\partial t^2} = 0, \tag{3.6}$$

whose solution has the form

$$\mathbf{A}(\mathbf{r},t) = \mathbf{A}_0\ e^{i(\mathbf{k}\cdot\mathbf{r}-\omega t)} + c.c.\ , \tag{3.7}$$

where $c.c.$ stands for complex conjugate, $\mathbf{k}$ is the wave vector and ω is the angular frequency of the optical field.

The first approximation to be made is the dipole approximation, aiming ultimately at neglecting the spatial variation of the vector potential over the extent of the atom, i.e. $\mathbf{A}(\mathbf{r},t) \approx \mathbf{A}(t)$. This is justified by arguing that, under usual experimental conditions, the atomic length scale (a few angstroms) is considerably smaller than the optical wavelenght (400 to 700 nm in the visible spectrum). Mathematically, the idea is expressed by $\mathbf{k}\cdot\mathbf{r} \ll 1$, and the vector potential $\mathbf{A}$ is then spatially uniform over the studied zone.

With this in mind, we return to the equation 3.5. As first consideration, the external electric field is defined as $\mathbf{E}(t) = -\ \partial\mathbf{A}(t)/\ \partial t$ in the Coulomb gauge. Second, we identify $e\ \mathbf{r}$ as the electric dipole moment, which in quantum mechanics is represented by the dipole moment operator $\mathbf{d}$. Therefore, the Hamiltonian describing the interaction of an electron bonded to an atom in the presence of an external classical electromagnetic field, under the dipole approximation, is given by

$$H(\mathbf{r},t) = \underbrace{\frac{\mathbf{p}^2}{2m} + V(r)}_{H_0} - \mathbf{d}\cdot\mathbf{E}(t) \tag{3.8}$$

where we have dropped the prime notation. The first two terms correspond to the Hamiltonian of the electron in the absence of the external field (usually referred to as the free Hamiltonian H_0), while the third term essentially depicts its interaction with the single-mode radiation.

The most important things to highlight from the last equation are the structure of the Hamiltonian and the mathematical expression for the interaction term. From here on, the next step to reach the Jaynes-Cummings Hamiltonian will be to fully quantize the previous model, which implies the quantization of the electromagnetic field. Although the exact expressions will be different, the Jaynes-Cummings Hamiltonian will be of the form

$$H_{JC} = \underbrace{H_{\text{atom}} + H_{\text{field}}}_{H_0} + H_{\text{int}}. \tag{3.9}$$

There are several ways to achieve the goal of the quantization of the electromagnetic field, but the one we will follow is the expanssion of the vector potential in terms of cavity modes [65], whereby the problem is reduced to the quantization of the harmonic oscillator corresponding to each individual mode of the cavity.

For a single-mode of the radiation field inside an optical cavity, and remembering that we have established the Planck unit system as standard, the electric field operator is given by

$$\mathbf{E} = \underbrace{\left(\frac{\omega_c}{V}\right)^{1/2} \sin(kz)}_{\equiv\, \lambda} \left(a + a^\dagger\right) \ , \tag{3.10}$$

where ω_c and k are the angular frequency and the magnitud of the wave vector of the mode, respectively, while V is the physical volume of the cavity and z is a spatial parameter that will have no relevance when applying the dipole approximation, since we must remember that under this approximation the spatial dependence for the field is ignored. For the sake of notational simplicity, all the parameters are absorbed into another parameter λ. It is worth mentioning that the unitary polarization vector has not been written explicitly as it is not necessary in the study of the single-mode field in a linear optical cavity.

In addition, $a^\dagger$ and a are the creation and annihilation operators satisfying the bosonic commutation relation $[a, a^\dagger] = 1$, whose physical meaning can be interpreted as the creation or destruction of a quantum of energy or, in other words, a photon. Let $|n\rangle$ represente the field state with n quanta of energy, then

$$a\,|n\rangle = \sqrt{n}\,|n-1\rangle \qquad (\ a\,|0\rangle = 0\ )\ , \tag{3.11}$$

and

$$a^\dagger\,|n\rangle = \sqrt{n+1}\,|n+1\rangle\ . \tag{3.12}$$

Under this quantization, the Hamiltonian associated solely with the single-mode electromagnetic field is

$$H_{\text{field}} = \omega_c\, a^\dagger a\ . \tag{3.13}$$

Here the constant term $\omega_c/2$ related to the vacuum field (also known as zero-point energy [66]) has been ignored because it does not contribute to the dynamics of the system beyond a global phase with no physical relevance. In the present single-mode analysis it is easy to get rid of this term by a simple energy shift, but for multi-mode systems, renormalization techniques must be considered [67]. Besides, by making the identification of $a^\dagger a$ as the number operator and ω_c as the energy of a single photon, the above expression makes sense for being the proper Hamiltonian to describe the energy of the field.

With respect to the atom, we have made the strong assumption that it is a system of only two energy levels, which are referred to as ground and excited states and are represented by $|g\rangle$ and $|e\rangle$, respectively. Let E_g be the energy of the ground state and E_e the energy of the excited state. We choose the midpoint between them $(E_e - E_g)/2$ as the zero energy. Moreover, we define their energy difference as ω_a, which is also a frequency in our choice of unit system. In this way, the Hamiltonian associated solely with the atom is

$$H_{\text{atom}} = \frac{\omega_a}{2}|e\rangle\langle e| - \frac{\omega_a}{2}|g\rangle\langle g|\ . \tag{3.14}$$

Next, the dipole moment operator $\mathbf{d} = e\,\mathbf{r}$, previously defined in the semiclassical formulation, acts on the atomic states. To find its representation in the basis of $|g\rangle$ and $|e\rangle$, one has to take into account that the position operator $\mathbf{r}$ has odd parity, which means that under an inversion transformation, the operator changes to $-\mathbf{r}$ [68]. This implies that $\langle e|\mathbf{d}|e\rangle = 0 = \langle g|\mathbf{d}|g\rangle$, and therefore, the operador $\mathbf{d}$ is only described by off-diagonal terms

$$\mathbf{d} = d\,|e\rangle\langle g| + d^*\,|g\rangle\langle e|\ , \tag{3.15}$$

where the parameter d can be assumed to be real without loss of generality. In this stage, it is also convenient to introduce the Pauli matrix $\sigma_z \equiv |e\rangle\langle e| - |g\rangle\langle g|$, and additionally the so-called atomic transition operators $\sigma_+ \equiv |e\rangle\langle g|$ and $\sigma_- \equiv |g\rangle\langle e|$, which satisfy the commutation relation

$$[\sigma_+, \sigma_-] = \sigma_z \,, \tag{3.16}$$

$$[\sigma_z, \sigma_\pm] = 2\sigma_\pm \,. \tag{3.17}$$

The operator σ_+ captures an excitation process of the atom since $\sigma_+|g\rangle = |e\rangle$, while σ_- captures an de-excitation process since $\sigma_-|e\rangle = |g\rangle$. This is the reason why they are call the transition atomic operators. With this in mind, the previous expressions reduce to

$$H_{\text{atom}} = \omega_a \frac{\sigma_z}{2} \,, \tag{3.18}$$

and

$$\mathbf{d} = d\,(\sigma_+ + \sigma_-) \,. \tag{3.19}$$

It is interesting to note that the Pauli matrix formalism, which initially arose in the context of quantum systems with spin 1/2, is likewise suitable for the analysis of the atomic system with only two energy levels. The reason for this is that the two systems are mathematically isomorphic [69], as well as any other system with only two accessible states (this generalization usually referred to as *qubit*). This is also partly why Rabi's work could be succesfully extrapolated to another, seemingly different physical context.

Returning to the construction of the model, we only need to describe the Hamiltonian that describes the interaction between the atom and the radiation field. For this purpose, we are going to use the interaction term already present in equation 3.8, but now in the formalism of the second quantization

$$H_{\text{int}} = -\,\mathbf{d}\cdot\mathbf{E} = \frac{\Omega}{2}\,(\sigma_+ + \sigma_-)\,(a + a^\dagger) \,, \tag{3.20}$$

where the minus sign and the parameters λ and d have been absorbed into Ω, which recieves the name of Rabi frequency and represents the strength of the coupling system-environment.

To reveal something more about the terms of this previous equation, it is a good idea to make a transformation to the interaction picture (where the Hamiltonian is denoted by $\tilde{H}_{\text{int}}$) with respect to $H_0 = H_{\text{atom}} + H_{\text{field}}$, resulting in

$$\tilde{H}_{\text{int}} = \frac{\Omega}{2}\left[a\sigma_-\, e^{-i(\omega_a+\omega_c)t} + a^\dagger\sigma_+\, e^{i(\omega_a+\omega_c)t} + a\sigma_+\, e^{-i(\omega_a-\omega_c)t} + a^\dagger\sigma_-\, e^{i(\omega_a-\omega_c)t}\right] \,. \tag{3.21}$$

We have obtained exponential terms that depend on the sum (quickly rotating terms) and the difference (slowly rotating terms) between the frequencies ω_a and ω_c, the first frequency being associated with the atomic transition energy and the second with the energy of the bosonic field mode. The disregard of the rapidly rotating terms constitutes what is known as the rotating wave approximation (abbreviated RWA) [70]. This is a valid approximation when the driving external electromagnetic field is near in resonance with the atomic transition frequency, and it is grounded in the fact that the fast oscillating terms couples states of large energy difference, whose transition is very unlikely to take place and therefore negligible for short enough times.

Returning to Schrödinger's picture and including the results for the free Hamiltonians of the atom and field, we finally obtain the total Hamiltonian of the Jaynes-Cummings model

$$H_{\text{JC}} = \omega_c\, a^\dagger a + \omega_a \frac{\sigma_z}{2} + \frac{\Omega}{2}\left(a\sigma_+ + a^\dagger\sigma_-\right) . \tag{3.22}$$

Note that the bosonic operators a and $a^\dagger$ act only on the number states $|n\rangle$ of the optical field, while the atomic transition operators σ_+ and σ_- act on the states $|g\rangle$ and $|e\rangle$. It is therefore natural to think that the

products of operators $a\sigma_+$ and $a^\dagger\sigma_-$ will act on the composed states $|g,n\rangle \equiv |g\rangle \otimes |n\rangle$ and $|e,n\rangle \equiv |e\rangle \otimes |n\rangle$. The state $|g,n\rangle$ ($|e,n\rangle$) corresponds to the atom being in the ground (excited) state in the presence of a single-mode radiation field with n *quanta* of energy or, to put it in another way, n photons. These states are usually referred to as *bare* in order to distinguish them from the energy *eigenstates* of the Jaynes-Cummings Hamiltonian 3.22, which are usually referred to as *dressed*.

Besides, the effect of the interaction Hamiltonian is to generate transitions only between states $|e,n\rangle$ and $|g,n+1\rangle$. In this order of ideas, the Jaynes-Cummings Hamiltonian can be represented as a block diagonal matrix, each block being a 2×2 matrix in the subspace spanned by $|e,n\rangle$ and $|g,n+1\rangle$, with $n \geq 0$

$$H^{(n)} = \begin{bmatrix} n\omega_c + \frac{\omega_a}{2} & \frac{\Omega}{2}\sqrt{n+1} \\ \\ \frac{\Omega}{2}\sqrt{n+1} & (n+1)\omega_c - \frac{\omega_a}{2} \end{bmatrix}, \tag{3.23}$$

whose energy eigenstates, denoted by $|n,\pm\rangle$ and known as dressed states, are given in term of the bare states by

$$|n,+\rangle = \cos\left(\frac{\theta_n}{2}\right)|e,n\rangle + \sin\left(\frac{\theta_n}{2}\right)|g,n+1\rangle\,, \tag{3.24}$$

$$|n,-\rangle = \sin\left(\frac{\theta_n}{2}\right)|e,n-1\rangle - \cos\left(\frac{\theta_n}{2}\right)|g,n+1\rangle\,, \tag{3.25}$$

with θ_n defined as

$$\theta_n = \tan^{-1}\left(\frac{\Omega\sqrt{n+1}}{\Delta}\right)\,, \tag{3.26}$$

being $\Delta \equiv \omega_a - \omega_c$ the detuning.

Finally, the energy eigenvalues are given by

$$E_n^{\pm} = \omega_c\left(n+\frac{1}{2}\right) \pm \frac{1}{2}\underbrace{\sqrt{\Delta^2 + \Omega^2(n+1)}}_{\equiv\Omega_n}\,, \tag{3.27}$$

where the generalized Rabi frequency Ω_n has been introduced.

The comparison between the energy scales of the bare and dressed states is presented in an illustrative manner in Figure 3.1. We note that $|g,0\rangle$ is the only bare states that is also a dressed state. Moreover, it is the energy eigenstate of minimun energy. Another thing to note is that, for each subspace characterized by n, the energy difference between the dressed states increases with this value, while the difference between the bare states is constant.

3.2 DYNAMICAL BEHAVIOR

As explained in Section 2.1, the most general approach for solving the dynamics of an open quantum system is to start from the von Neumann equation for the density matrix of the composed system (whose evolution is unitary), and then trace over the environmental degrees of freedom. The follow-up of this procedure leads to, in principle, an expression for the time evolution of the reduced density matrix concerning only the system of interest.

The complexity of the resulting equations of motions is usually overwhelming in most cases, but there are some simple quantum systems for which exact solutions are known to exist. This is the exceptional

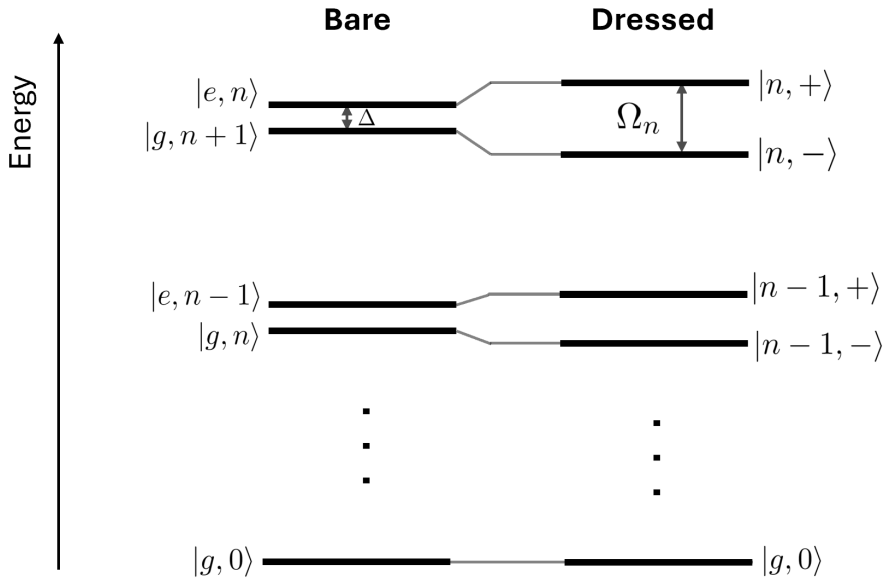

Figure 3.1: Comparison between the bare and the dressed states for the Jaynes-Cummings model in terms of the values of energy. Here it is clearly observed that the Hamiltonian of the model couples the states $|e,n\rangle$ and $|g,n+1\rangle$, where $n \geq 0$. As a first observation, it should be pointed out that the state $|g,0\rangle$ is the only bare state which is also a dressed state, and it is moreover the state with the minimum energy of the model. On the other hand, the energy difference between the dressed states belonging to the same subspace is increasing with the value of n, in contrast with the constant energy difference between the corresponding bare states.

case for the JCM. Taking advantage of this fact we will follow a different approach here based on the well-known time evolution for the probability amplitudes describing the state of the composed system (atom coupled to radiation field). In addition, apart from obtaining more compact expressions, these solutions also represent a major benefit from the point of view of numerical implementation, since the computation times are significantly reduced in comparison to those associated with solutions provided by the general approach.

The construction of the state of the composed system is as follows. Consider the initial atomic state as an arbitrary quantum superposition of the ground $|g\rangle$ and excited $|e\rangle$ energy *eigenstates* of the atom

$$|\psi(0)\rangle_{\text{atom}} = c_g(0)\,|g\rangle + c_e(0)\,|e\rangle, \tag{3.28}$$

where the normalization condition $|c_g(0)|^2 + |c_e(0)|^2 = 1$ has to be fulfilled. In the same spirit, the initial field state is taken to be an arbitrary superposition of the Fock basis

$$|\psi(0)\rangle_{\text{field}} = \sum_{n=0} c_n(0)\,|n\rangle. \tag{3.29}$$

Under the assumption that at the initial instant of time there are still no correlations between the atomic system and the environment, the initial state of the composed system can be expressed as a tensor product of the atom and field states

$$\begin{aligned} |\Psi(0)\rangle &= |\psi(0)\rangle_{\text{atom}} \otimes |\psi(0)\rangle_{\text{field}} \\ &= \sum_{n=0} \left[\underbrace{c_g(0)c_n(0)}_{\equiv c_{g,n}(0)}\,|g,n\rangle + \underbrace{c_e(0)c_n(0)}_{\equiv c_{e,n}(0)}\,|e,n\rangle \right]. \end{aligned} \tag{3.30}$$

It is worth noting that the construction of the composed state from this tensor product is not valid in general for arbitrary times. Immediately after the initial instant, the subsystems are allowed to interact with each other and therefore entanglement is expected to emerge [3], making the mathematical description of the state not so trivial in terms of non-separable probability amplitudes

$$|\Psi(t)\rangle = \sum_{n=0} [\, c_{g,n}(t)\, |g,n\rangle + c_{e,n}(t)\, |e,n\rangle \,]\,. \tag{3.31}$$

Now, keeping in mind that the coupling Hamiltonian allows transitions only between the states $|e,n\rangle$ and $|g,n+1\rangle$, it is convenient to rewrite the previous equation as

$$|\Psi(t)\rangle = c_{g,0}(t)\, |g,0\rangle + \sum_{n=0} [\, c_{e,n}(t)\, |e,n\rangle + c_{g,n+1}(t)\, |g,n+1\rangle \,] \tag{3.32}$$

and solving the dynamics for each subspace spanned by $|e,n\rangle$ and $|g,n+1\rangle$, with $n \geq 0$.

Before solving the time evolution problem, an additonal consideration must be taken. Note that when analyzing the energy spectrum provided by the Jaynes-Cummings Hamiltonian, the minimum energy value is linked entirely to the energy *eigenstate* $|g,0\rangle$, for which the atom is in its ground state and the radiation field is in a vacuum state (no photons). This is the only bare state that is also an energy eigenstate, and this occurs because it is not subject to the processes of absorption or emission of radiation, therefore no transitions to other states occur. Then, bearing in mind that a shift in the values of energy does not change the dynamical solution beyond a global phase with no physical relevance, it is desirable to set the lowest energy value equal to zero. In this way, we can ignore the state $|g,0\rangle$ in the state expansion 3.32 since it does not contribute to the time evolution of the composed state in this new energy scale.

By inserting the composed state expanssion into the Schrödinger equation in the interaction picture, a couple set of differential equations is obtained for the probability amplitudes. Its solution is well known [71] subject to certain initial conditions and is provided by

$$\begin{aligned} c_{e,n}(t) &= \left\{ c_{e,n}(0) \left[\cos\left(\frac{\Omega_n t}{2}\right) - \frac{i\Delta}{\Omega_n} \sin\left(\frac{\Omega_n t}{2}\right) \right] - c_{g,n+1}(0) \frac{2ig\sqrt{n+1}}{\Omega_n} \sin\left(\frac{\Omega_n t}{2}\right) \right\} e^{i\Delta t/2}, \\ c_{g,n+1}(t) &= \left\{ c_{g,n+1}(0) \left[\cos\left(\frac{\Omega_n t}{2}\right) + \frac{i\Delta}{\Omega_n} \sin\left(\frac{\Omega_n t}{2}\right) \right] - c_{e,n}(0) \frac{2ig\sqrt{n+1}}{\Omega_n} \sin\left(\frac{\Omega_n t}{2}\right) \right\} e^{-i\Delta t/2}, \end{aligned} \tag{3.33}$$

where $\Delta = \omega_a - \omega_c$ is the detuning, $g = \Omega/2$ is a parameter that, like the Rabi frequency Ω, quantifies the strength of the interaction, and $\Omega_n^2 \equiv \Delta^2 + 4g^2(n+1)$ is the generalized Rabi frequency.

The above equation is the most general one, but it is particularly easier to focus on the resonant case characterized by $\Delta = 0$, for which $\Omega_n = 2g\sqrt{n+1}$. In this scenario, the dynamics of the probability amplitudes is reducible to

$$\begin{aligned} c_{e,n}(t) &= c_{e,n}(0)\, \cos\left(g\sqrt{n+1}\, t\right) - i\, c_{g,n+1}(0)\, \sin\left(g\sqrt{n+1}\, t\right), \\ c_{g,n+1}(t) &= c_{g,n+1}(0)\, \cos\left(g\sqrt{n+1}\, t\right) - i\, c_{e,n}(0)\, \sin\left(g\sqrt{n+1}\, t\right). \end{aligned} \tag{3.34}$$

Keeping in mind that the main objective of the present work is not to solve the Jaynes-Cummings dynamics, but to apply on this model the technique that will be introduced to characterize the non-Markovianity of the system. In this sense, the resonant case has no special relevance other than being the simplest from the numerical point of view for what we want to demonstrate.

At this stage, the temporal evolution of the composed state is completely identified by knowing the dynamics

of its probability amplitudes. It is useful now to employ the density matrix formalism to retrive the atomic state information from the partial trace over all the degrees of freedom of the environment. For it we take into account that the composed state is a pure state, and consequently, its matrix density is constructed in the simple manner $\rho(t) = |\Psi(t)\rangle\langle\Psi(t)|$. The reduced density matrix concerning only the atom is then

$$\rho_{\text{atom}}(t) = \begin{bmatrix} \rho_{gg}(t) & \rho_{ge}(t) \\ \rho_{eg}(t) & \rho_{ee}(t) \end{bmatrix} = \begin{bmatrix} \sum_{n=0} |c_{g,n+1}(t)|^2 & \sum_{n=0} c_{g,n+1}(t)\, c^*_{e,n+1}(t) \\ \sum_{n=0} c^*_{g,n+1}(t)\, c_{e,n+1}(t) & \sum_{n=0} |c_{e,n}(t)|^2 \end{bmatrix}. \tag{3.35}$$

This result is very powerful, because with it one can know in detail the time evolution of any initial condition of the atomic state and of the light state considered. Let's take a closer look at two examples of interest: i) an atom in the excited state in absence of photons and ii) an atom in the ground state interacting with a coherent state of light.

3.2.1 Example I: Excited and Vacuum States

The initial atomic state is just $|e\rangle$, while the initial field state is just $|0\rangle$. In terms of the initial probability amplitudes, the only one different from zero is $c_{e,0} = 1$. This implies that the reduced density matrix of the atom results in

$$\begin{bmatrix} \sin^2(gt) & 0 \\ 0 & \cos^2(gt) \end{bmatrix}, \tag{3.36}$$

where only $n = 0$ has contributed to the summation of equation 3.35.

The diagonal terms of the reduced density matrix are referred to as the atomic populations. By populations we mean the probability of obtaining a certain result when performing a measurement, and is associated with the Copenhagen interpretation of the wave function [72]. From the statistical point of view, this means that when preparing an assembly with many identical systems and performing a measurement on each of them, the quotient between the number of times a result was obtained and the total number of systems prepared is defined as the probability of obtaining that specific result when performing a measurement. It is natural then to assert that the populations take values between zero and one, and that the sum of them must be exactly equal to one, in agreement with the properties of the density matrix. In the present case, ρ_{gg} (ρ_{ee}) corresponds to the probability that when a measurement is performed in the basis $\{|g\rangle, |e\rangle\}$, the atom is found to be in the ground (excited) state for a given instant of time.

Hence, the probability P_e of obtaining the state $|e\rangle$ when performing a projective measurement is shown in the Figure 3.2. The interesting thing to note here is that even though there are no photons present, the atom is still subject to processes of emission and absorption of radiation, since the probability P_e varies in time. This phenomenon, known as Rabi oscillations [73], is caused by the coupling of the excited atom with the vacuum fields, which results in the process of spontaneous emission and subsequent reabsorption of the emitted photon. This result cannot be predicted by the semiclassical light-matter interaction theory, since it predicts that transition between atomic states are no posible when no external fields are present.

3.2.2 Example II: Ground and Coherent States

In this other example, the initial composed state is given by

$$|\Psi(0)\rangle = |g\rangle \otimes |\alpha\rangle = \sum_{n=0} \underbrace{e^{-\frac{|\alpha|^2}{2}} \frac{\alpha^n}{\sqrt{n!}}}_{c_{g,n}(0)=c_n(0)} |g, n\rangle\,, \tag{3.37}$$

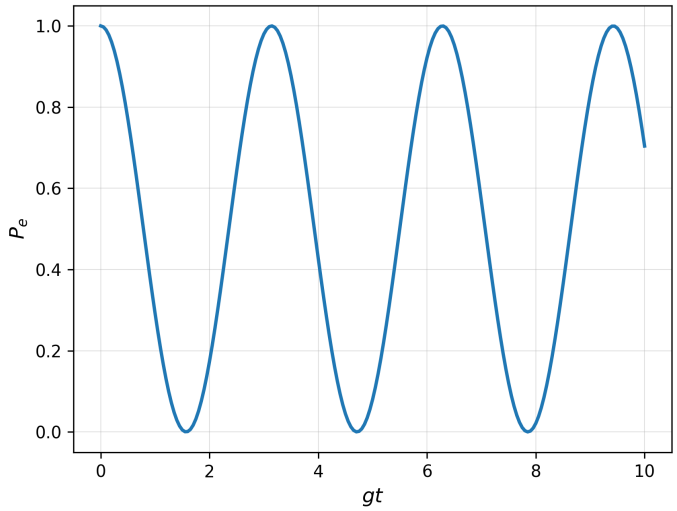

Figure 3.2: Dynamical behavior of the probability (also population) P_e of finding the atom in its excited energy state when a projective measurement is performed, taking as initial state an exicted atom and a vacuum radiation field in resonance. The spontaneous emission and subsequent reabsorption of the emitted photon is known as the Rabi vacuum oscillations. Besides, it has to be mentioned that in the Planck system of units, the quantity gt is dimensionless.

where α is a complex parameter characterizing the so-called coherent state of light [74], with $|\alpha|^2 = \bar{n}$, being $\bar{n}$ the average number of photons present in the radiation field.

In this particular case, we are going to consider a photon field with average number $\bar{n}$ equal to 25. What's more, in order to simplicity the numerical treatment, we will assume the parameter α to be real, so that the amplitude probabilities becomes $c_n(0) = e^{-\bar{n}/2}\sqrt{\bar{n}^n/n!}$, in such a way that the probabilities $P_n = |c_n|^2$ follow a Poisson-type distribution [75], as illustrated in Figure 3.3. Although in principle the sum is infinite, it is clear that not all terms c_n contribute significantly to the construction of the initial composed state. Therefore, we can make a truncation in the number of terms taken into account based on the information provided by Figure 3.3.

Now, making use of equation 3.35, the dynamical behavior is calculated subject to the initial conditions given by equation 3.37. At this stage, we will not be looking at the populations P_e nor P_g for the atomic state (associated with ρ_{ee} and ρ_{gg}, respectively), but rather at the so-called population inversion w defined as

$$w(t) = \rho_{gg}(t) - \rho_{ee}(t) \ , \tag{3.38}$$

which gives us information about the relative difference between populations of the ground and excited atomic states.

The dynamics of $w(t)$ is pictured in the Figure 3.4. It can be viewed that the population inversion exhibits an oscillating behavior and its envelope, in the first instance, seems to follow a decay of exponential type. This first phenomenon is known as a collapse, and has a respective associated collapse time τ_c given by [71]

$$\tau_c = \frac{1}{g\sqrt{2}} \ , \tag{3.39}$$

which is intrinsic to the model as it is independent of the average number of photons present in the radiation field. From its dependence on the coupling parameter g, it can be said that the stronger the coupling, the faster the collapse occurs.

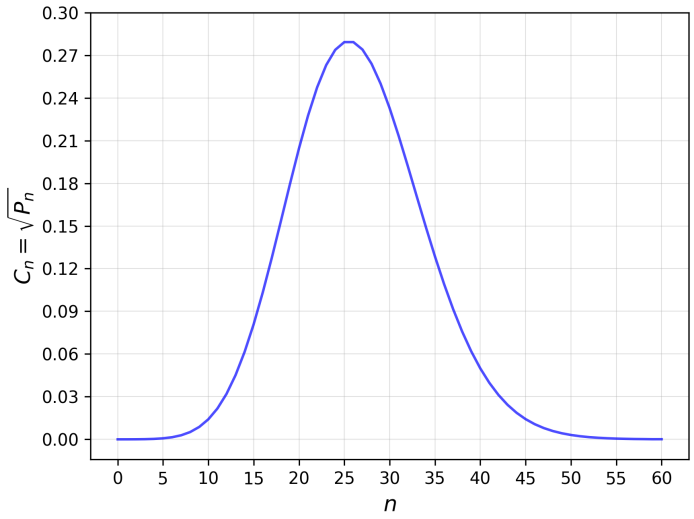

Figure 3.3: Poisson-type distribution followed by the probabilities $P_n = |c_n|^2$ describing a coherent state of light with average photon number $\bar{n} = 25$. Based on this graph, the truncation of the number of terms considered for the correct description of the coherent state is done

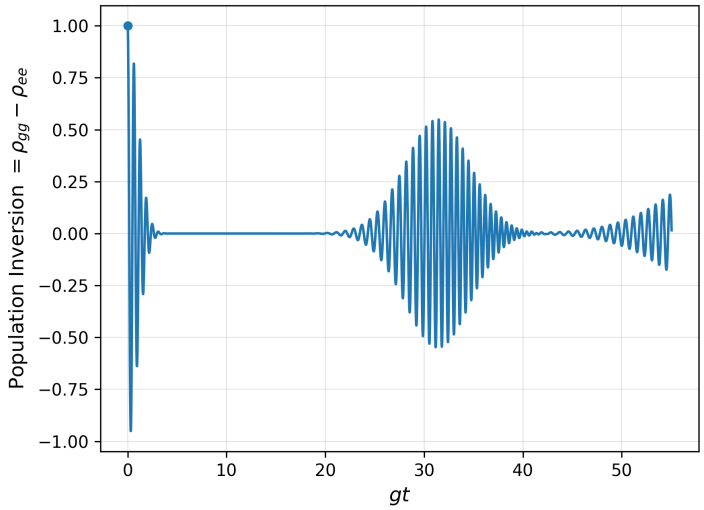

Figure 3.4: Dynamical behavior of the quantity known as population inversion, taking as initial composed state an atom in its ground state and a coherent light state in resonance with average photon number $\bar{n} = 25$, where its value at $t = 0$ has been highlighted in the graph. This behavior is usually referred to as quantum beats, and encompasses the processes of collapse and revival of atomic populations, the latter being one of the main differences between the semiclassical and the fully quantized model for radiation-matter interaction.

After collapse, the function w remains constant equal to zero, until this changes surprisingly when the oscillating behavior becomes present again in the evolution. This phenomenon is extremely interesting and is known as the revival of atomic populations. One could see it as a memory effect (characteristic of non-Markovian systems), where the future evolution of the system does not depend exclusively on the immediately preceding time, but all its past history must be taken into account. There is also an associated

characteristic revival time τ_r (the time to wait until the revival is observed) given by

$$\tau_r = \frac{2\pi}{g}\sqrt{\bar{n}}\ . \tag{3.40}$$

In contrast to the collapse time τ_c, the revival time τ_r has dependence on the average number of photons with which the atom is free to interact. In this sense, the characteristics of the environment itself play a crucial role in whether or not the revival phenomenon is observed. For very large environments in the sense of the average number of photons, one must wait a long time to appreciate the revival such that, in praxis, the studied system exhibits no memory effects. This is in accordance with the ideas of the memoryless Markovian approach, where one of the physical conditions for its validity is a large size of the environment compared to that of the system, such that the former is not appreciably affected during the coupling and therefore there would only be an irreversible loss of information from the system to the environment.

Notwithstanding, the above comment regarding the flow of information must be handled with care when applied to population inversion. Although the population inversion gives us insight into the certainty that we would obtain a result when performing a projective measurement on the basis $\{|g\rangle, |e\rangle\}$, and therefore $w = 0$ could be interpreted as the inability to predict the result, i.e. absence of information, we must also consider that $\{|g\rangle, |e\rangle\}$ is not the only existing basis for the description of the problem, and therefore the information could be contained in other different states. Nonetheless, it is worth mentioning that there are very specific cases where population inversion does serve for this purpose, but this does not mean that the idea can be extrapolated to the general case. On the other hand, there exist other physical quantities that can be interpreted as suitable information quantifiers instead of w, such as for example the purity of the quantum state. The corresponding discussion will be adressed later in the following section.

What is important to mention and make very clear is that the revival phenomenon presented by the JCM can be associated to a non-Markovian dynamics, whose most characteristic feature is the memory effects. Accordingly, the JCM is of great interest for our objective in the present work in order to apply the technique that will be presented in Chapter 4 on a non-Markovian system.

3.3 BLOCH SPHERE REPRESENTATION

According to equation 3.28, at the initial instant of time, the atomic state corresponds to a pure quantum state written as an arbitrary coherent superposition of the base atomic states $|g\rangle$ and $|e\rangle$.

It is now convenient to introduce an alternative way of representing geometrically the pure states of a two-level system (a qubit) in a so-called Bloch sphere representation, whose name refers to the scientist Felix Bloch, who although not being the one who introduced this representation, it bears his name in honor of his advances in quantum mechanics [76]. The representation is given in the present context by

$$|\psi(0)\rangle_{\text{atom}} = \cos\frac{\theta}{2}\,|g\rangle + e^{i\varphi}\sin\frac{\theta}{2}\,|e\rangle\ . \tag{3.41}$$

This means that the quantum pure state is parameterized only by the two real variables θ and φ, instead of by two complex probability amplitudes c_g and c_e. This has advantages from a computational point of view, but also as a visualization tool for the states and their dynamics. Here, θ and φ have the usual meaning of angles and take values in the ranges $0 \leq \theta \leq \pi$ and $0 \leq \varphi \leq 2\pi$, respectively. In this way, physical states can be represented geometrically as points on the surface of the so-called Bloch sphere, where each point represents a unique physical state and vice versa. This can be clarified by looking at the Figure 3.5. For example, $\theta = 0$ corresponds to $|g\rangle$ while $\theta = \pi$ corresponds to $|e\rangle$, located at opposite poles on the sphere. Note that for the above two values of θ, the value taken by φ is irrelevant, but $\varphi = 0$ is usually chosen for ease. For other possible values of θ, the value of φ needs to be specified.

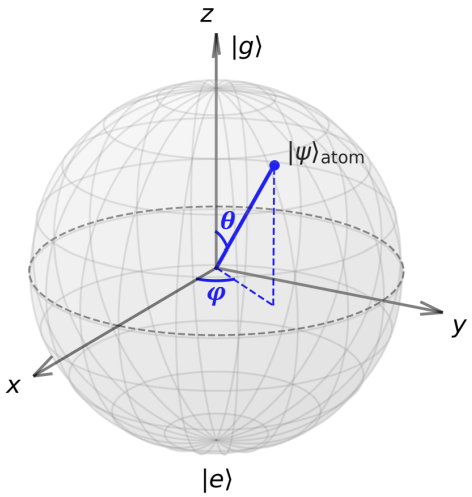

Figure 3.5: Representation of pure quantum state on the surface of the so-called Bloch sphere. This is valid for two-level systems (also referred to as qubits). The two orthogonal states that constitute the base are located at two opposite poles of the sphere.

In this manner, the initial composed state of the atom coupled to the radiation field, given by equation 3.32, can be rewritten as

$$|\Psi(0)\rangle = \sum_{n=0} \left[\underbrace{e^{i\varphi} \sin\frac{\theta}{2}\, c_n}_{c_{e,n}(0)} \; |e,n\rangle + \underbrace{\cos\frac{\theta}{2}\, c_{n+1}}_{c_{g,n+1}(0)} \; |g,n+1\rangle \right], \tag{3.42}$$

where it must be clear that the coefficients c_n $(n \geq 0)$ refer to the initial state of the field.

By then applying the known equations 3.34 for the time evolution of the probability amplitudes in the resonant case and the equation 3.35 for the construction of the reduced density matrix from these, we obtain the dynamical behavior for any initial condition of the atom only by specifying the values of θ and φ. The interesting thing is that from this reduced density matrix, we can also find the representation in the Bloch sphere of the state at times posterior to the initial one. This is obtained by specifying the three cartesian coordinates of the Bloch vector $\mathbf{v} = (u, v, w)$ from the four components of the reduced density matrix

$$u(t) = \rho_{eg}(t) + \rho_{ge}(t) = \langle \sigma_x(t) \rangle \,, \tag{3.43}$$

$$v(t) = i\,[\,\rho_{ge}(t) - \rho_{eg}(t)\,] = \langle \sigma_y(t) \rangle \,, \tag{3.44}$$

$$w(t) = \rho_{gg}(t) - \rho_{ee}(t) = \langle \sigma_z(t) \rangle \,, \tag{3.45}$$

where all result in real quantities, which are identical to the expected value of the Pauli operator of their respective spatial direction. In particular, the quantity w is exactly equal to the population inversion employed previously; therefore, the z component of the Bloch vector gives us the value of this quantity. In this representation, addiationally, the components of the x and y directions associated with the off-diagonal terms of the density matrix play here an equally important role as the z component. In this order of ideas, the Bloch sphere representation provides more information about the system than that obtained by limiting ourselves to the population inversion.

On the other hand, the pure atomic states (in particular the initial state) are represented by points on

the surface of the sphere as already mentioned. However, it may happen that when plotting the resulting state given by the density matrix as a point on the Bloch sphere representation, it can be located at points inside the surface of the sphere. This is a very frequent scenario since the state resulting from the time evolution usually corresponds to a mixed state due to the correlations built in its coupling with the environment. In this direction, the Bloch sphere representation also provides us with visual tools to differentiate between pure states (on the surface) and mixed states (inside). This is based on the fact that the purity of a quantum state, define as $\mathrm{Tr}(\rho^2)$, must fullfill $\mathrm{Tr}(\rho^2) \leq 1$, where the equality is satisfied by only pure states [1].

Now, in relation to the discussion on the Markovianity (or not) of the system, the transition from the initially pure state to a mixed state can be interpreted as a loss of information from the system to the environment as a product of its coupling. As already discussed in Chapter 2, when the state is pure we know exactly and completely the coefficients of the coherent superposition, while when the state is mixed we have only partial information about the state. Hence, the presence of a revival in the time evolution of purity can be correctly interpreted as a backflow information from the environment to the system, not like in the analysis made with the population inversion.

Let us now visually exemplify the dynamical behavior of a particular state in the Bloch sphere representation to get an idea of its use. In the current case, we consider the initial atomic state as $|+\rangle = (|g\rangle + |e\rangle)/\sqrt{2}$, which is parameterized by $\theta = \pi/2$ and $\varphi = 0$; and the initial field state as a coherent state with average number of photons $\bar{n} = 9$. The evolution was considered up to twice the revival time τ_r. The dynamics is illustrated in Figure 3.6. The chosen state $|+\rangle$ has a very interesting property, since when the average number of photons of the coherent state is very large, this atomic state remains at all times very close to the surface of the sphere, thus remaining almost always pure [77].

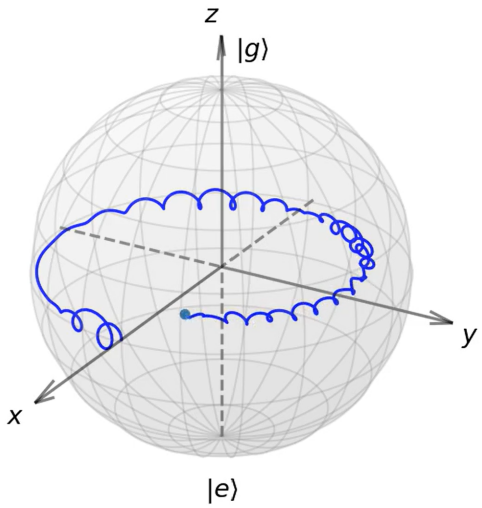

Figure 3.6: Dynamical behavior in the Bloch sphere representation of the initial $|+\rangle = (|g\rangle + |e\rangle)/\sqrt{2}$ atomic state coupled to an initial coherent field state with average photon number $\bar{n} = 9$. The dynamics was calculated up to twice the revival time τ_r. The point represents the final state.

This same procedure can be applied to any initial state to visualize its temporal evolution on the Bloch sphere. The next step will be to consider a set of points uniformly distributed over the surface of the sphere, seeking to represent as many initial states on the sphere as possible. By analyzing their collective evolution we will be able to find a behavior perhaps unimaginable if the analysis were done point by point separately.

In the following, the methodology proposed for the selection of the points that will serve as initial conditions will be described. First, it is necessary to make the obvious comment that given the discrete nature of the

computational processes, it is not possible to choose the points continuously. It then becomes fundamental to decide also the number of points necessary for a reliable description of the problem and to avoid falling into unnecessary overcomputation that would lengthen the computation times. The procedure is as follows:

1. Uniformly discretize the parameters θ and φ in their intervals, i.e. π and 2π, respectively. Here we will denote $\Delta\theta$ and $\Delta\varphi$ as the steps in each interval.

2. The surface of the sphere will be divided into horizontal circles labeled by the values of the variable θ, as shown in the Figure 3.7. In order that the points are more or less evenly distributed, it is natural to think that the circles with the longest length are also the ones with the most points. This implies that the size of the step $\Delta\theta$ is fixed in principle, while $\Delta\varphi$ is different for each horizontal circle. Therefore, the step $\Delta\varphi'$ in each circle will depend on the number of points $N_{\theta'}$ present, such that $\Delta\varphi' = \frac{2\pi}{N_{\theta'}}$.

3. The horizontal circle along the equator of the sphere is the one with the longest length. This will be taken as a reference and we will choose that it has a total of N points. In this way, $\Delta\varphi_{\text{equ}} = \frac{2\pi}{N}$ is an ammount fixed by us by choosing the value of N.

4. The quotient between the number of points and the length of the circumference is required to be a constant to achieve a uniform distribution. The length of the equator circle is 2π, while the other circles have a length $C' = 2\pi \sin\theta'$ and $N_{\theta'}$ points. It follows that $\frac{N}{2\pi} = \frac{N_{\theta'}}{2\pi \sin\theta'}$, which implies $N_{\theta'} = N \sin\theta'$. As a result $\Delta\varphi' = \frac{2\pi}{N \sin\theta'}$.

5. In order to also achieve uniformity in the vertical direction with respect to the rest of the sphere, it is required that $\Delta\theta = \Delta\varphi_{\text{equ}}$. Moreover, under the condition that the equator of the sphere is a reachable value for θ (otherwise the above assertions are meaningless), it is required $\Delta\theta$ to be a divisor of $\pi/2$, which implicates that $\Delta\varphi_{\text{equ}}$ as well fulfills this condition. Mathematically this means that $\frac{\pi/2}{\Delta\varphi_{\text{equ}}}$ must be an integer number, where it should be remembered that $\Delta\varphi_{\text{equ}} = \frac{2\pi}{N}$.

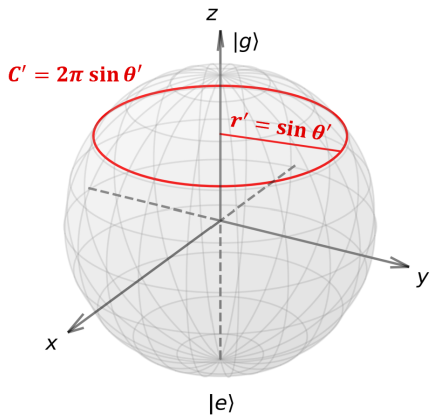

Figure 3.7: Length of the circumference C' of an arbitrary horizontal circle as a function of angle θ. The horizontal circles are expected to have a number of points according to its length, in order to achieve a more or less uniform distribution of points on the surface of the Bloch sphere.

With all these considerations, the possible choices for the value of N are

$$N = 4n \quad , \quad \text{with} \;\; n \geq 1 \;\in\; \mathbb{N}. \tag{3.46}$$

In Figure 3.8 a comparison between different spheres of initial conditions for different choices of N is shown, mentioning also the number of total points on the sphere.

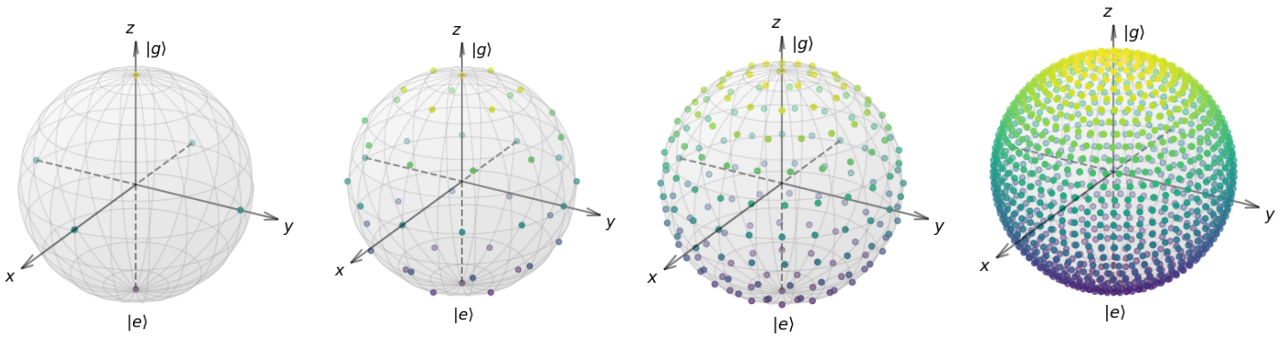

(a) $N = 4,$ Points $= 6.$ (b) $N = 12,$ Points $= 46.$ (c) $N = 24,$ Points $= 184.$ (d) $N = 60,$ Points $= 1148.$

Figure 3.8: Sphere of initial conditions for different values of N (defined as the number of points on the equator). The number of total points considered on the surface of the sphere for each case is also included.

In particular, the value of $N = 24$ (184 points in all on the sphere) seems to us an appropriate choice both to elucidate the dynamics of the full sphere of points and to avoid excessively long computation times. The decision of this choice will be justified in the next chapter when we will see the influence that the number of points considered has on the values obtained by our proposal for a non-Markovianity quantifier, which will also be presented in the next chapter. For the time being, the collective dynamics of the initial conditions sphere is illustrated in the Figure 3.9, where the atom is coupled to a radiation field characterized by coherent state with an average number of photons $\bar{n} = 9$ and its evolution is shown at eight given instants in terms of the revival time τ_r. It should be noted that these snapshots were taken from an animation we made (which is available to be shared if desired).

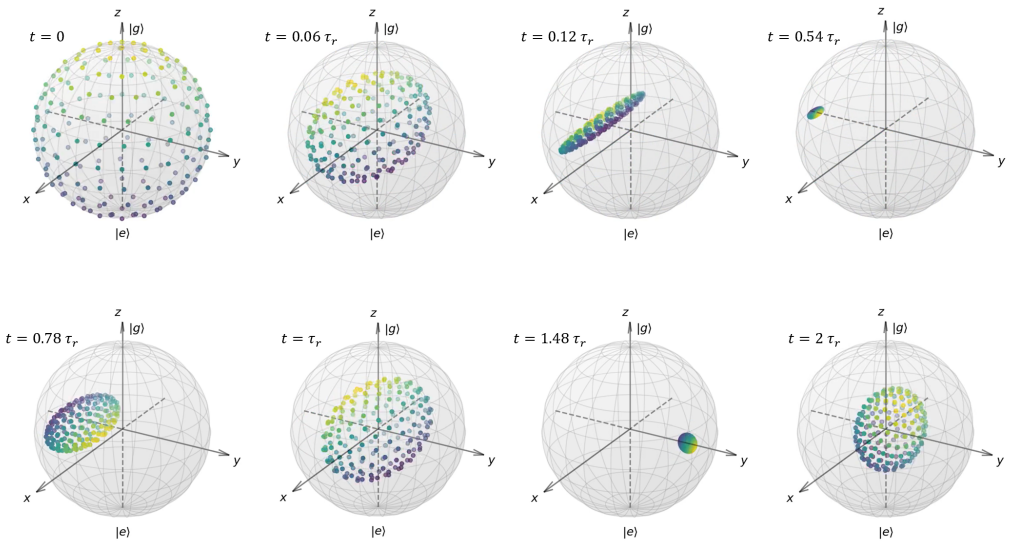

Figure 3.9: Evolution of the sphere of initial conditions when the atom is coupled to a radiation field described by a coherent state of light with mean number of photons equal to $\bar{n} = 9$. The collective dynamics was calculated from the initial instant $t = 0$ up to twice its revival time $t = 2\tau_r$, and geometrically represented by an animation, from which these eight configurations were extracted as snapshots.

The first instants correspond to the collapse phenomenon, where the sphere of initial conditions is first flattened forming an ellipsoid, then a line and finally a single point. With respect to this last collective state (corresponding to time $t = 0.54\tau_r$ in this example), it indicates that the Jaynes-Cummings model can be used as an instrument for the preparation of quantum states, since every point regardless of its position on the initial sphere converges to that particular state [78]. We must also remember that the z component of

each point in this representation gives us the value of the population inversion, which we discussed earlier (see Figure 3.4 for example). Thus this way of visualizing the time evolution of the atomic states is more complete, since the data concerning the difference between the populations of the ground and excited states can be extracted from only one of the Cartesian coordinates.

After the collapse, the revival phenomenon is observed, here represented as an increase in the volume of the ellipsoid of points trying to return to its initial configuration on the surface of the sphere. This can be interpreted as a backflow of information from the environment to the atomic system, since the loss of information contained in the system could be seen as a reduction in the distinguishability between the quantum states when the volume is reduced, even becoming all totally indistinguishable from each other in certain instant of time. Therefore, the return of distinguishability and the attempt to return to the initial states configuration on the sphere is interpreted as the recovery of the information that the system had previously lost. This is precisely a signature of a non-Markovian system.

CHAPTER 4

Retrieving non-Markovianity from PCA

In recent years, the amount of data handled in society has grown steeply, mainly due to technological progress and digitalization [79]. The amount is such that it is often overwhelming and discouraging to study them. Because of this, the area of data analysis research has gained relevance in recent years, offering collection, cleaning, transformation and modeling techniques, with the main objective of discovering useful information about the data that, at first glance, seems indecipherable. In this way, conclusions and interpretations can be drawn about the data being handled. Physics is no stranger to this trend, and the implementation of data analysis and machine learning techniques have gained relevance in modern research topics [80–86]. In this specific work, we will implement a technique known as principal component analysis (PCA) in the proposal of a non-Markovianity quantifier.

4.1 PRINCIPAL COMPONENT ANALYSIS

Principal component analysis (abbreviated PCA) is a data analysis technique whose main objective is to decompose high-dimensional data into its most statistically descriptive factors [87]. It is based on a matrix decomposition method known as singular value decomposition (abbreviated SVD). The PCA consists of applying the SVD to a preprocessed data set, which is made up of the mean-subtracted original data with variance set equal to one.

Data are usually presented in the form of matrices. In an image, for example, the information of each pixel that composes it may be contained in the elements of a matrix, or, as another example, in a series of measurements, each column of the matrix may represent a set of experimental data obtained at a precise instant of time. In this order of ideas, we will call $\mathbf{X}$ the matrix containing all the data we want to analyze. Let $\mathbf{X} \in \mathbb{C}^{n\times m}$ be a complex-valued matrix of size $n \times m$ written in the form

$$\mathbf{X} = \begin{bmatrix} | & | & & | \\ \mathbf{x_1} & \mathbf{x_2} & \cdots & \mathbf{x_m} \\ | & | & & | \end{bmatrix}. \tag{4.1}$$

We normally deal with a large amount of information, so it is to be expected that the size of the $\mathbf{X}$ matrix can become very large. This is referred to as high-dimensional data. Such a large amount of data is naturally overwhelming, but techniques have been developed for their processing and analysis, such as the singular value decomposition (SVD).

The SVD consists of performing a matrix decomposition that always exists for complex-valued matrices and

that is unique. It is written as

$$\mathbf{X} = \mathbf{U}\mathbf{\Sigma}\mathbf{V}^{\dagger} \, , \tag{4.2}$$

being $\mathbf{U} \in \mathbb{C}^{n\times n}$ and $\mathbf{V} \in \mathbb{C}^{m\times m}$ unitary matrices with orthonormal columns, and $\mathbf{\Sigma} \in \mathbb{R}^{n\times m}$ a diagonal real-valued matrix with non-negative entries. The columns of $\mathbf{U}$ are called left singular vectors of $\mathbf{X}$ and the columns of $\mathbf{V}$ are right singular vectors. The diagonal elements of $\mathbf{\Sigma}$ are called singular values. A characteristic feature of this decomposition is that the singular values are arranged in a decreasing order.

This technique can be associated to the solution of a problem of eigenvalues and eigenvectors of the correlation matrices $\mathbf{X}\mathbf{X}^{\dagger}$ (which relates the data of the rows of $\mathbf{X}$) and $\mathbf{X}^{\dagger}\mathbf{X}$ (which relates its columns). Both matrices have the same eigenvalues, and we identify the square root of these with the singular values contained in $\mathbf{\Sigma}$. On the other hand, the eigenvectors of the matrix $\mathbf{X}\mathbf{X}^{\dagger}$ are precisely the columns of $\mathbf{U}$, while the same happens with the columns of $\mathbf{V}$ as eigenvectors of the matrix $\mathbf{X}^{\dagger}\mathbf{X}$. In this sense, the unitary matrices $\mathbf{U}$ and $\mathbf{V}$ contain the information concerning the correlation in the columns and rows of $\mathbf{X}$, respectively. In addition, the fact that the singular values are ordered from highest to lowest indicates a hierarchical ordering in the $\mathbf{U}$ and $\mathbf{V}$ matrices. This means that the columns of $\mathbf{U}$ (left singular vectors) are ordered according to how much correlation they capture from the columns of $\mathbf{X}$, while the columns of $\mathbf{V}$ (right singular vectors) are also ordered hierarchically according to the correlation they contain about the rows of $\mathbf{X}$.

Following this perspective, one of the most important application of SVD is to reduce the dimensionality of a matrix by truncating the number of singular values taken into account, thus obtaining what is known as a low-rank approximation. This is based on the fact that the hierarchical ordering indicates that the first terms will always be those that contain the most statistical descriptive factors about the matrix under study, and in contrast, the last terms are those that contain the most irrelevant statistical information about it. Some of its best known applications are [88] image compression, noisy data processing, pseudo-inverse computation for non-square matrices, least-squares, regressions, among others.

Knowing at this point the SVD, it is time to explain the PCA technique. The PCA consists of applying the SVD to a set of data after they have been standardized, which means that their average value is subtracted to set their mean equal to zero (so that the data is centered at the origin of the respective coordinate system) and their variance is set equal to 1. This is important to ensure that all variables describing the data (which for example may represent physical quantities different from each other such as time and temperature) contribute equally to the calculation of the principal components.

Furthermore, it is a common practice to consider only the $\mathbf{U}$ and $\mathbf{\Sigma}$ matrices in the decomposition, since the former provides information on the directions of maximum variance in the data (which are contained in its columns and are referred to as principal components), while the latter provides the magnitude of the variance in each direction. These principal components, denoted PC from now on, are hierarchically ordered and are mutually orthogonal. Moreover, the PCs constitute a new coordinate system in which the visualization and interpretation of the data is more convenient, since it allows capturing a large part of the information about the data in the first coordinates. The PCA is usually implemented in dimensionality reduction and compression problems, denoising, pattern recognition and classification problems, among others [89, 90].

A very important feature of PCA (also of SVD) is that the dominant statistical patterns are deciphered directly from the data provided, without the need for intuition or prior knowledge of what they represent. Herein lies the power and great applicability of this technique to any type of problem in a wide variety of study topics. In particular, we will apply the PCA to the set of quantum states of an atom in its coupling with a radiation field, which are geometrically depicted by the reduced density matrix of the atom in the Bloch sphere representation and whose evolution falls within the description of the Jaynes-Cummings model.

4.2 PCA AS A NON-MARKOVIANITY MEASURE

In this case, we will apply the PCA to the Bloch sphere configuration (see Section 3.3) at each time instant. Our data matrix $\mathbf{X}$ is then composed of the set of points in each snapshot, where each point is characterized by three spatial components and the number of total points N_T depends on the initial chosen distribution over the surface of the Bloch sphere (again refer to Section 3.3).

Therefore the dimension of $\mathbf{X}$ is $3 \times N_T$ for any given instant of time. By applying the PCA, we obtain that the $\mathbf{U}$ and $\mathbf{\Sigma}$ matrices of the decomposition both have dimension 3×3, indicating that there are three orthogonal directions (PCs) in which the variance of the data is maximal. This is to be expected since the Bloch sphere representation is a three-dimensional space. Moreover, the matrix multiplication of $\mathbf{U}$ with $\mathbf{\Sigma}$ results in the projection of the standarized data onto these particular directions (see Figure 4.1a). The blue line indicates the first principal component (denoted as PC1), which contains the most relevant statistical descriptive features of the data, while the red and black lines correspond to the second and third principal components (PC2 and PC3), respectively.

In particular, we use the Python *numpy* library function `linalg.svd` applied to the pre-processed data. Another option is to use the Python *scikit-learn* library. Below, a fragment of the code used to calculate the PCs is shown.

```
import numpy as np

# ...

u = np.empty( (len(t), len(phi) ) )   # "x" coordinates
v = np.empty( (len(t), len(phi) ) )   # "y" coordinates
w = np.empty( (len(t), len(phi) ) )   # "z" coordinates
# "len(t)" corresponds to the time interval &
# "len(phi)" is the number of points in each snapshot

# ... (calculation of u,v,w)

P = np.empty(( len(t), 3, len(phi) ))  # Array of points
P_avg = np.empty(( len(t), 3 ))        # To compute the mean (centroid)
B = np.empty(( len(t), 3, len(phi) ))  # Mean-substracted data
U = np.empty( (len(t), 3, 3) )         # SVD decomposition: Matrices U & S
S = np.empty( (len(t), 3) )
length = np.empty( (len(t), 3) )       # Principal Components (PC)

for s in np.arange(len(t)).astype(int):
    P[s] = np.array( [u[s,:], v[s,:], w[s,:]] )
    P_avg[s] = np.mean( P[s], axis=1 )
    B[s] = P[s] - np.tile( P_avg[s], ( len(phi), 1 ) ).T
    #SVD
    U[s], S[s], VT = np.linalg.svd( B[s] / np.sqrt( len(phi) ), full_matrices=0 )
                    # the "square root" is for setting the variance equal to 1
    for i in range(0,3):
        lx = 0; ly = 0; lz = 0
        lx = U[s][0,i] * S[s][i]    # "x" component of the PC
        ly = U[s][1,i] * S[s][i]    # "y" component of the PC
        lz = U[s][2,i] * S[s][i]    # "z" component of the PC
        length[s][i] = np.sqrt( lx**2 + ly**2 + lz**2 )
```

Nonetheless, for our concrete purpose of correctly interpreting the PCs on a physical ground, it is necessary

to scale the lengths of these projections by some factor to fairly match the original data rather than the standardized data. One way to accomplish this is to determine the appropriate scale factor from the initial configuration at $t = 0$, when all points are on the surface of the Bloch sphere and it is clear that the proper length of each PC in this configuration must be exactly equal to 1 in order to match the set of points. This obtained scaling factor is fixed and will then be applied to each of the three PCs from any configuration at later times (see Figure 4.1b for a time $t \neq 0$). This is achieved by modifying the last part of the previous code, where the matrix multiplication of $\mathbf{U}$ with $\mathbf{\Sigma}$ should be rescaled and thus so is the length of the vectors representing the PCs. Below, a fragment of the modified code is shown.

```
scale = 1/length[0,0]   # where the length of the first PC at t=0 is used
# We could use the length of the second (length[0,1]) or third (length[0,2]) PC as well,
# since they are all equal at t=0.

for s in np.arange(len(t)).astype(int):
    # ... (repeat exactly the same code as before for the SVD decomposition)

    for i in range(0,3):
        lx = 0; ly = 0; lz = 0
        lx = U[s][0,i] * scale * S[s][i]
        ly = U[s][1,i] * scale * S[s][i]
        lz = U[s][2,i] * scale * S[s][i]
        length[s][i] = np.sqrt( lx**2 + ly**2 + lz**2 )
```

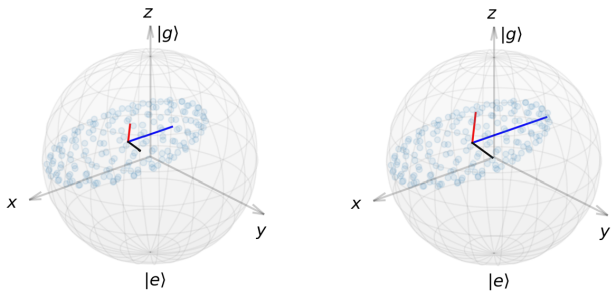

(a) (b)

Figure 4.1: Example of the application of PCA to a snapshot of the time evolution of the atom that is coupled to a coherent light field with mean number of photons $\bar{n} = 9$ in the JCM. The number of points considered for constructing our data matrix was 184, which corresponds to the choice of $N = 24$ in equation 3.46. In one side, (a) is the direct result given by the PCA, while (b) is the resultant after scaling the lengths of the projections according to the initial configuration to match the original data.

For plotting the PCs on the Bloch sphere, the data preprocessing for the SVD is undone in the code below.

```
import matplotlib.pyplot as plt

fig = plt.figure(figsize=(6,6))
ax = fig.add_subplot(111, projection='3d')

# ...

sc = ax.scatter([], [], [], alpha=0.1)
PC1, = ax.plot([], [], [], '-', color='blue')
```

```
PC2, = ax.plot([], [], [], '-', color='red')
PC3, = ax.plot([], [], [], '-', color='black')

r = 10   # time index

sc._offsets3d = (P[r][0, :], P[r][1, :], P[r][2, :])

PC1.set_data_3d([P_avg[r][0], P_avg[r][0] + U[r][0, 0] * scale * S[r][0]],
                [P_avg[r][1], P_avg[r][1] + U[r][1, 0] * scale * S[r][0]],
                [P_avg[r][2], P_avg[r][2] + U[r][2, 0] * scale * S[r][0]])

PC2.set_data_3d([P_avg[r][0], P_avg[r][0] + U[r][0, 1] * scale * S[r][1]],
                [P_avg[r][1], P_avg[r][1] + U[r][1, 1] * scale * S[r][1]],
                [P_avg[r][2], P_avg[r][2] + U[r][2, 1] * scale * S[r][1]])

PC3.set_data_3d([P_avg[r][0], P_avg[r][0] + U[r][0, 2] * scale * S[r][2]],
                [P_avg[r][1], P_avg[r][1] + U[r][1, 2] * scale * S[r][2]],
                [P_avg[r][2], P_avg[r][2] + U[r][2, 2] * scale * S[r][2]])
```

The idea now is to apply the rescaled PCA to each configuration associated to each time instant (see Figure 4.2) and to keep track of the dynamics of the respective lengths PC1, PC2 and PC3 (see Figure 4.3). Associating the present analysis with the discussion carried out at the end of Section 3.3, it is possible to interpret the decrease of the PCs as a loss of information from the system to the environment, and consequently, its subsequent growth with a blackflow of information from the environment to the system. From this point of view, the representation on the Bloch sphere helps us a lot to visualize geometrically the evolution in the JCM and the subsequent application of the PCA, but the real relevant information about memory effects (signature of non-Markovianity) is found in the temporal evolution of the PCs.

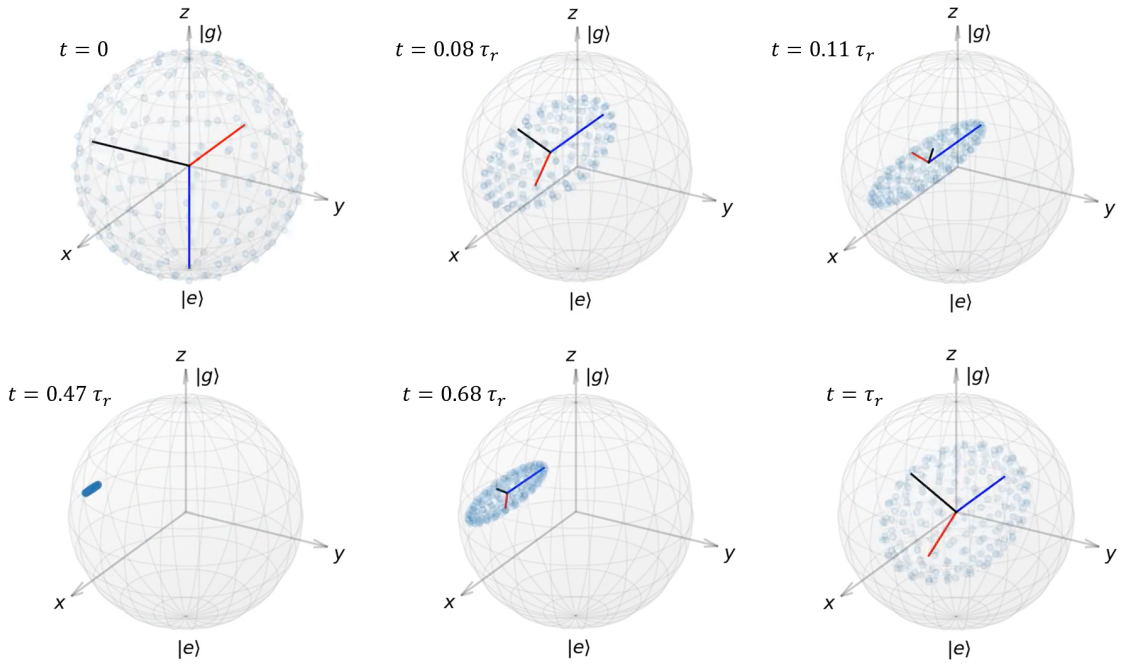

Figure 4.2: Rescaled PCA applied to some selected snapshot of the evolution of the Bloch sphere representation of the atomic states in the JCM. Here we considered the coupling radiation field to be a coherent state with average photon number $\bar{n} = 9$ and a total of 184 points for representing the sphere of initial conditions.

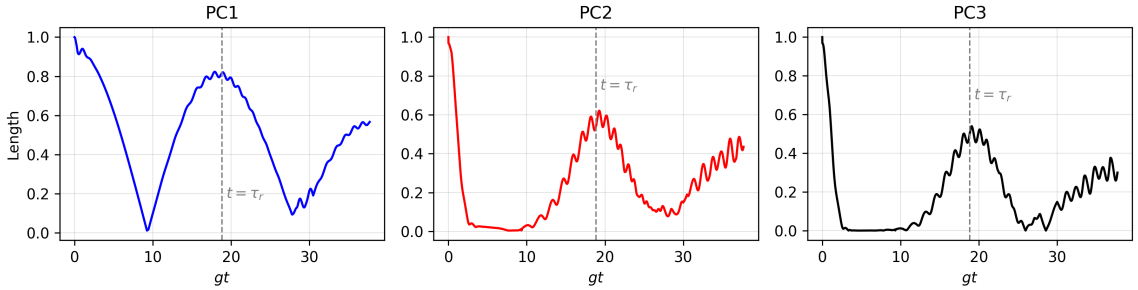

Figure 4.3: Time evolution of the lengths of the three principal components associated with Figure 4.2. Recall that gt is a dimensionless quantity, where g is a parameter that quantifies the strength of the system-environment coupling. In this particular case the value $g = 0.1$ was chosen for completeness of the numerical implementation, but the choice of this value has no further justification than this.

Here is where our proposal to quantify the non-Markovianity of an open quantum system is born. As just mentioned, the growth of the PCs is interpreted here as a characteristic feature of non-Markovianity, but more important is its rate of change with respect to time, since a faster growth of the PCs would indicate that the transfer of information back into the system is accomplished more quickly, and thus more non-Markovian the system would be. In this direction, we define the rates of change with respect to time of the principal components PC1, PC2 and PC3 as

$$\xi_i = \frac{d}{dt} PC_{(i)} \ , \qquad i = 1, 2, 3 \ . \tag{4.3}$$

As a next step, we will focus on all time intervals where the PCs are increasing (characterized by $\xi_i > 0$) and we will take the cumulative contribution of the growth of the three PCs as a quantifier or measure of the non-Markovianity $\mathcal{N}_{\text{PCA}}$ of the system. This is written as

$$\mathcal{N}_{\text{PCA}} = \sum_{i=1}^{3} \int_{\xi_i > 0} \xi_i \, dt \ . \tag{4.4}$$

In this approach, the three projections of the data in the directions of greatest variance (represented here by the three PCs) all contribute to the calculation of the quantifier $\mathcal{N}_{\text{PCA}}$. This is a characteristic feature of our approach and we regard it as important, because although the PCs are ranked in hierarchical order with respect to the statistical variance of the data, this does not imply a hierarchical order also with respect to the rate of change of their lengths. Thus, it is necessary to include the rate of change of the three PCs so as not to ignore important contributions to the quantifier.

Another very important feature to take into account is that our proposal does not involve the solution of a maximization problem, which is very demanding from the computational point of view and is one of the major disadvantages of some of the non-Markovianity measure methods presented in Chapter 2. From the numerical point of view, the application of PCA does not require many computational resources, since one of its main uses (although not in the present case) is dimensionality reduction. It is usual then that PCA is also applied to high-dimensional data matrices, so the technique has been optimized in the last decades to be quite efficient, and here we take advantage of this remarkable calculation performance.

Let us now perform the calculation of our proposed non-Markovian quantifier to the dynamics of an atom coupled to a coherent field of light described by the Jaynes-Cummings model. We must first review the issue of the number of points we must consider in the sphere of initial conditions (see Figure 3.8). Since we are applying a data analysis method, it is essential to be clear on how the choice and number of data forming the matrix we want to analyze affects the results obtained. The ideal would be to consider

all possible pure states of the atom, but obviously this is absurd given the discrete nature of numerical processes. Therefore, it is necessary to choose a number of initial conditions that gives reliable results and does not imply an overcomputation.

In the Table 4.1 different values for $\mathcal{N}_{\text{PCA}}$ were calculated by considering a coherent field with mean number of photons $n_{\text{mean}} = 9$ and then with $n_{\text{mean}} = 25$. The calculations were repeated varying the number of initial conditions considered in each case. It should be noted that the relevant parameters for the calculation in the Planck unit system were $t_{\text{initial}} = 0$, $t_{\text{final}} \approx 386$ (twice the revival time τ_r for $n_{\text{mean}} = 9$), $dt = 0.1$ and $g = 0.1$.

Number of Points	$\mathcal{N}_{\text{PCA}}$, $n_{\text{mean}} = 9$	$\mathcal{N}_{\text{PCA}}$, $n_{\text{mean}} = 25$
6	5.23	2.86
22	5.24	2.87
46	5.20	2.71
128	5.20	2.71
184	5.20	2.71
412	5.20	2.71
510	5.19	2.70

Table 4.1: Values for $\mathcal{N}_{\text{PCA}}$ under different average photon numbers (coherent field) and different number of initial points considered. The first two results are far from the results provided when considering a higher total number of points. From 46 points considered, the results obtained are almost identical.

According to our methodology for choosing the way in which the initial points are distributed on the sphere, the two options with the lowest number of points (according to those available to choose from) result in values of $\mathcal{N}_{\text{PCA}}$ that are far from the rest of the values for this quantifier. This is to be expected, since a low number of points does not guarantee the validity of the results obtained. On the other hand, the result obtained when considering a total of 46 points (corresponding to $N = 12$ in Figure 3.8) is almost identical to the results obtained when considering a larger number of points. Therefore, the choice of 46 points seems to us the most reasonable to optimize time and computational resources, and at the same time, obtain reliable results. Logically, these comments are valid only for the methodology proposed in Section 3.3. If another approach to choose the distribution is considered, the respective analysis must be performed.

Taking the above into account, we will choose 46 points to build our data matrix from here on. Now, we want to address the discussion of how our quantizer $\mathcal{N}_{\text{PCA}}$ varies as the average number of photons n_{mean} of the coherent light field varies. In this direction, Figure 4.4 shows a comparison of the time evolution of the principal components PCs for different values of the average number of photons (where $t_{\text{initial}} = 0$, $t_{\text{final}} \approx 700$, $dt = 0.1$ and $g = 0.1$ were defined).

The most evident feature of the Figure 4.4 is the decrease in the occurrence of the revivals phenomenon with increasing the average photon number. As a consequence, the non-Markovianity measure $\mathcal{N}_{\text{PCA}}$ is also reduced, as illustrated in Figure 4.5. This is an expected consequence, since when the size of the environment (understood as the number of degrees of freedom) is much larger than the size of the system, the former is not appreciably affected by the coupling and can be considered virtually constant, while the latter does change appreciably. This is a distinguishing feature of memoryless Markovian systems, which is reflected in the fact that the quantifier takes smaller and smaller values, until, for example, for a coherent field with $n_{\text{mean}} = 500$, the measure is almost equal to zero, indicating that there are no signs of non-Markovian behavior, i.e. a fully Markovian dynamics. This could also be inferred from the absence of

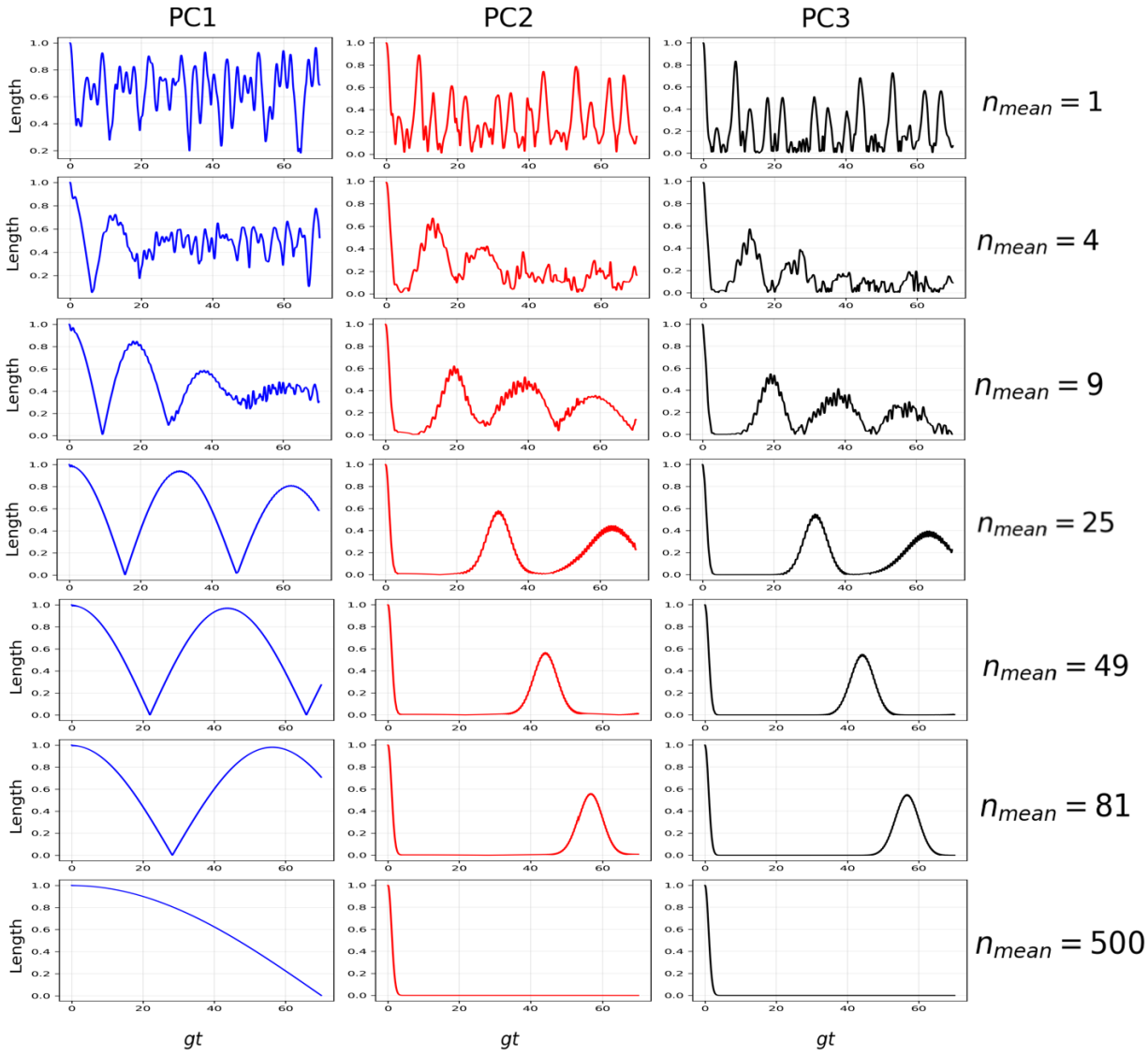

Figure 4.4: Time evolution of the three principal components PCs for different values of the average number of photons n_{mean} present in the coherent radiation field. The characteristic revivals of non-Markovian systems become less and less frequent as the average number of photons increases.

revivals in Figure 4.4 during the defined time interval.

As a complementary analysis, the choice of a normalized time scale will now be considered. In that case, one consistent choice is based on the revival time τ_r (see equation 3.40), whose value depends on the mean photon number of the radiation field. The dynamical evolution of the reduced density matrix of the atom is calculated from $t = 0$ to $t = 2\tau_r$ for each n_{mean}, taking a division of 2000 values evenly spaced in the time interval. The time evolution of the three PCs is illustrated in Figure 4.6 for different n_{mean} values. Similarly, the dependence of the non-Markovianity index $\mathcal{N}_{\text{PCA}}$ with the average photon number n_{mean} is depicted in Figure 4.7 in this normalized time scale.

With the exception of the first two plots, which correspond to $n_{\text{mean}} = 1$ and $n_{\text{mean}} = 4$, three general features are observed as the value of n_{mean} increases in Figure 4.6. First, the secondary oscillations around the mean PCs values become absent. Second, the peak value reached by PC1 is larger, which is not the case for PC2 and PC3. Third, the width of the revival peak becomes narrower and narrower for the

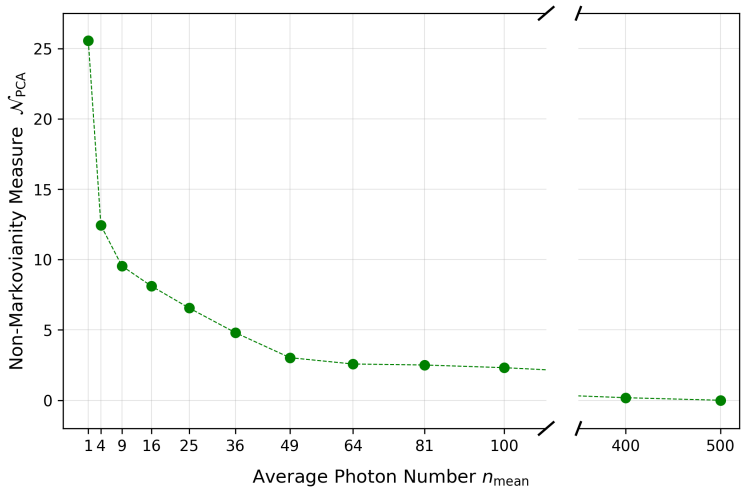

Figure 4.5: Values for the non-Markovianity measure $\mathcal{N}_{\text{PCA}}$ with respect to the average photon number n_{mean} characterizing the coherent state of light to which the atom is coupled. An important remark is that the same time interval has been taken for each n_{mean}. The inverse relationship indicates the loss of non-Markovian features as the environment becomes larger and larger. A value $\mathcal{N}_{\text{PCA}} = 0$ indicates a fully Markovian dynamics.

principal components PC2 and PC3.

Unfortunately, no general feature can be extracted in a simple way from Figure 4.7, where no obvious correlation between the data for $\mathcal{N}_{\text{PCA}}$ and n_{mean} is observed. One could argue that the lack of connection between the two data sets (as observed in Figure 4.5) could have its basis in the different choices for dt, which depends on the n_{mean} value. But, the calculations have also been performed for a fixed dt value, obtaining almost the same numerical values for $\mathcal{N}_{\text{PCA}}$ as before.

It should be noted at this point that, due to the discrete nature of computational calculations, the time evolution of quantum states (and therefore of PCs) is very sensitive to the choice of the dt value. However, once a sufficiently good time resolution is achieved, the same results are obtained for even smaller dt values. This is exactly what happens in the current situation, where a time division of 2000 values is good enough for a proper calculation of $\mathcal{N}_{\text{PCA}}$, even for the largest time interval related to $n_{\text{mean}} = 500$. Therefore, a smaller dt value does not change the already obtained results.

On the other hand, one could argue that the problem lies in the way of performing numerical derivatives of the time evolution data. Although different approaches have been taken into account (e.g. discrete derivatives and spline interpolation), almost the same numerical values were obtained in those cases as well. Based on those facts, it is concluded that the non-Markovian index $\mathcal{N}_{\text{PCA}}$ strongly depends on the time scale considered in the study.

Up to now, the discussion has been limited to the study of pure states as initial conditions, which are represented as points on the surface of the Bloch sphere. The reason for choosing this methodology is the straightforward functional form of the time evolution of the composed state (given by equations 3.34 and 3.35), which allows both greater clarity in the interpretation of the system dynamics, as well as extraordinary computational performance.

Nevertheless, the analysis can also deal with the choice of atomic initial conditions as mixed states. This is done in Appendix A. There it will be seen that the non-Markovianity index given by the PCA, taking a

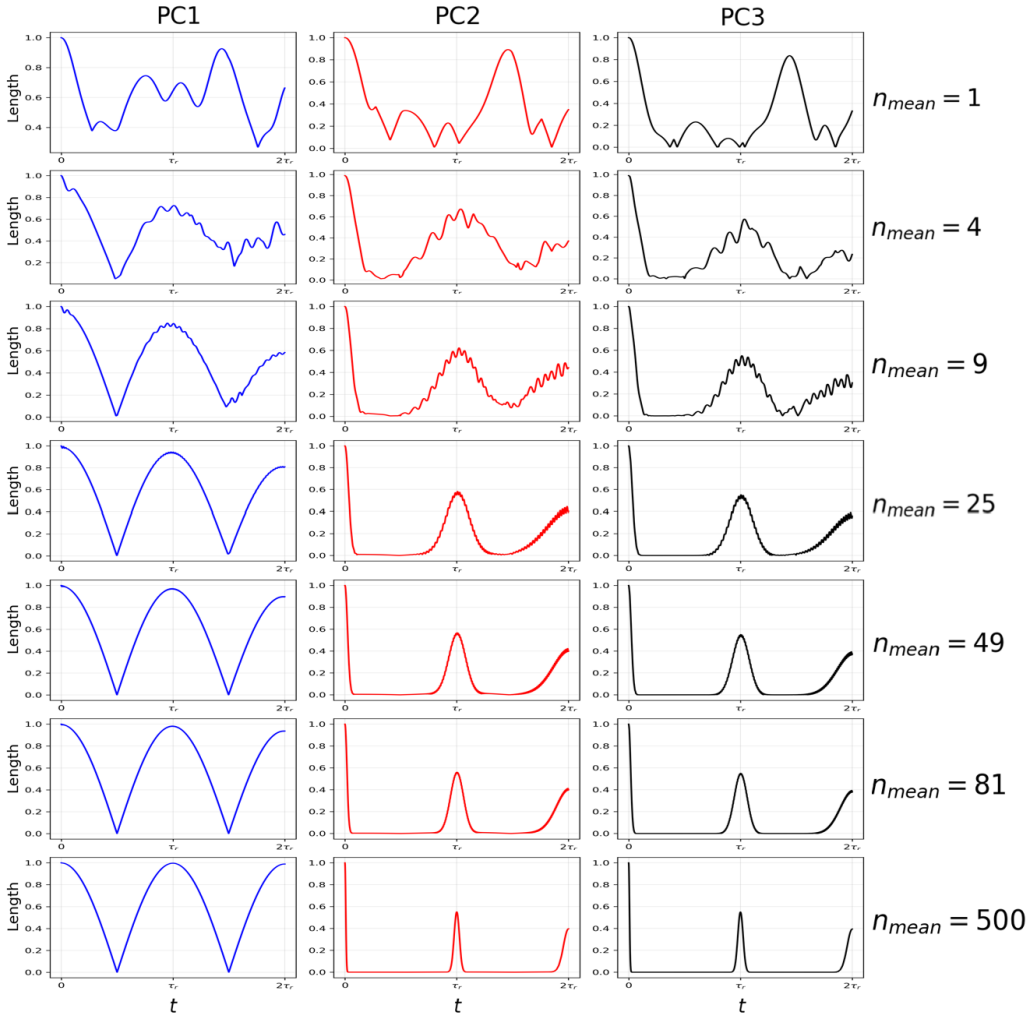

Figure 4.6: Time evolution of the three PCs for different values of the average number of photons n_{mean}. The time intervals are expressed in terms of the revival time τ_r, whose value is n_{mean}-dependent.

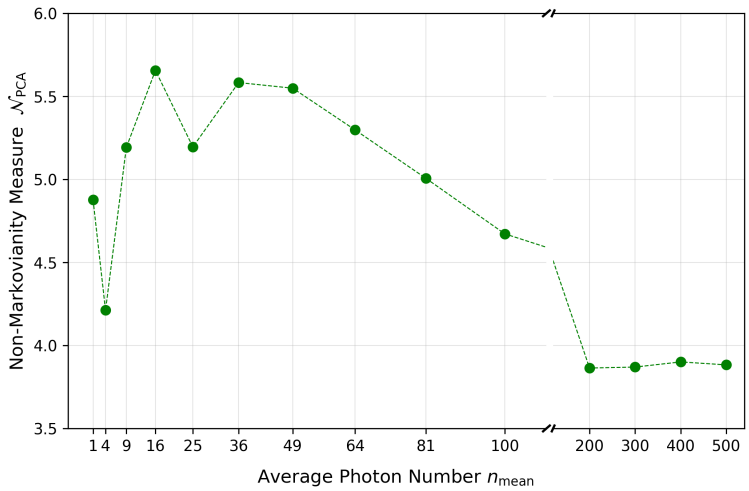

Figure 4.7: Values for the non-Markovianity measure $\mathcal{N}_{\text{PCA}}$ with respect to the average photon number n_{mean}, where a normalized time scale has been taken into account in terms of the revival time τ_r.

fixed n_{mean} value, is directly proportional to the radius of the sphere of initial conditions. This implies that by choosing mixed states instead of pure states, the index $\mathcal{N}_{\text{PCA}}$ is only rescaled by the radius of the initial sphere configuration, likewise the dynamical evolution of the PCs is also rescaled by the same factor.

4.3 COMPARISON OF OUR PROPOSAL WITH OTHER IDEAS AND APPROACHES

We shall now devote a large part of the present discussion to a qualitatively and quantitative comparison of our method with the most widely used method in the literature: the proposal of Breuer-Laine-Piilo (BPL) [16], which has already been presented in the equation 2.24. The first advantage of our method lies in, to paraphrase what has just been said, the low computational costs required for the calculation compared to BLP.

With respect to the optimization problem for the BLP measure, it must be performed between pairs of initial conditions. Although the optimization is restricted to quantum states only orthogonal to each other [40], the problem is still a challenging one. Consider that one has to calculate the integral of equation 2.24 for the evolution of all possible pairs of orthogonal initial conditions, and then determine which one has the maximum value, so as to finally obtain the non-Markovianity measure. In our method we apply the PCA to the whole configuration composed of all quantum states (on the Bloch sphere), without having to establish pairwise relations or anything like that, thus avoiding complications in the implementation of the method.

Another aspect to take into account is the fact that we are considering the contributions of all the three principal components PCs. We also consider that this is an advantage with respect to BLP, which only considers one direction given by the trace distance. This is related to the fact that the BPL measure is based on the evolution of only one pair of initial conditions, thus ignoring the contribution of the other possible quantum states. This does not seem adequate to us, because although the information on the evolution of the ideal pair of initial conditions is the one that gives the greatest measure of non-Markovianity in the whole time interval, it is also true that in certain time sub-intervals the ideal pair that maximizes the measure could differ, whose contribution is ignored in BLP. That is, the pair of optimal conditions may vary in time, being different from those found at the initial instant. In this aspect, we are certain that our method is preferable, since in addition to considering the analysis of the evolution of all the three directions that contain the greatest statistical variance in the data, the calculation of these directions is updated at each time instant or snapshot, making the results obtained more complete and general.

In addition to the qualitative discussion, the non-Markovianity index $\mathcal{N}_{\text{BLP}}$ was also calculated for each set of parameters (n_{mean} and time interval) discussed in the previous analyses. The results can then be directly compared with those already obtained using our proposal based on the PCA method. The results of the calculations of the non-Markovianity indices for different values of n_{mean}, taking the same time scale, are presented in Table 4.2. The $\mathcal{N}_{\text{PCA}}$ index is decomposed into its constituents $\mathcal{N}_{\text{PC1}}$, $\mathcal{N}_{\text{PC2}}$ and $\mathcal{N}_{\text{PC3}}$, where their sum must be equal to the $\mathcal{N}_{\text{PCA}}(\text{Total})$; while the $\mathcal{N}_{\text{BLP}}$ index is located in the last column of the table. On the other hand, Figure 4.8 shows the time evolution of the trace distance for the pair of initial conditions that are appropriate for the calculation of the $\mathcal{N}_{\text{BLP}}$ for different n_{mean} values.

Thus, a similarity is observed between the calculated values of $\mathcal{N}_{\text{PC1}}$ and $\mathcal{N}_{\text{BLP}}$ for values of $n_{\text{mean}} \geq 25$. This gives an indication that the time evolution of the first principal component PC1 corresponds precisely to the time evolution of the trace distance between the proper initial conditions for $\mathcal{N}_{\text{BLP}}$. This idea is reinforced by comparing the dynamics of PC1 in Figure 4.4 with the dynamics of the trace distance in Figure 4.8, again being very similar to each other. However, it is worth noting that this is true only for $n_{\text{mean}} \geq 25$. For these values, the appropriate pair of initial conditions corresponds to $|+\rangle$ and $|-\rangle$, where $|\pm\rangle = (|g\rangle \pm |e\rangle)/\sqrt{2}$; while for $n_{\text{mean}} < 25$, the appropriate pair changes to $|g\rangle$ and $|e\rangle$.

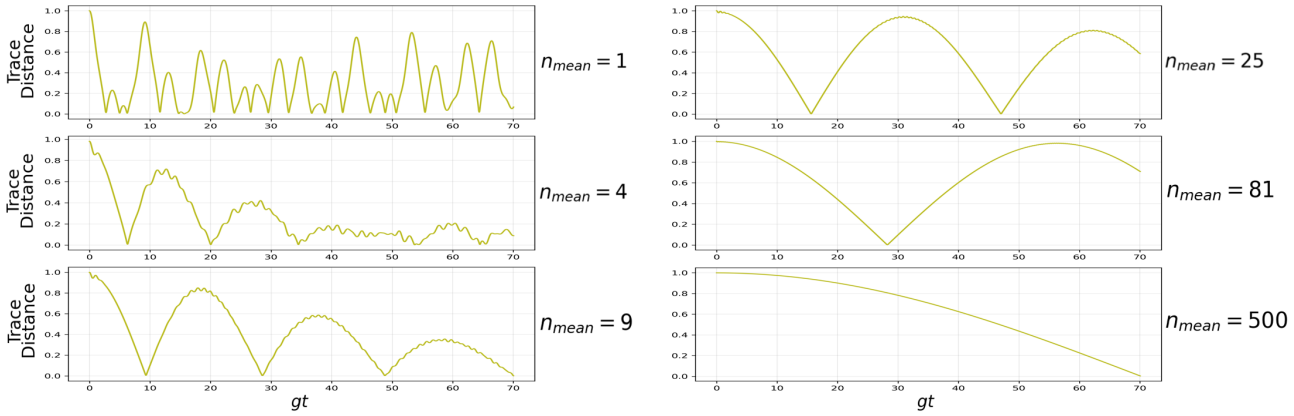

Figure 4.8: Time evolution of the trace distance between the proper pair of initial conditions that maximizes the non-Markovianity measure $\mathcal{N}_{\text{BLP}}$. Different values of the average number of photons n_{mean} present in the coherent radiation field were considered. An important remark is that the same time interval has been taken for each n_{mean}.

n_{mean}	$\mathcal{N}_{\text{PCA}}$ (Total)	$\mathcal{N}_{\text{PC1}}$	$\mathcal{N}_{\text{PC2}}$	$\mathcal{N}_{\text{PC3}}$	$\mathcal{N}_{\text{BLP}}$
1	25.56	8.61	8.56	8.39	19.77
4	12.43	5.25	3.63	3.55	23.37
9	9.55	3.09	3.02	3.44	14.99
16	8.12	2.55	2.81	2.76	7.03
25	6.56	2.35	2.13	2.08	2.31
36	4.81	1.81	1.54	1.46	1.77
49	3.03	1.30	0.89	0.83	1.29
64	2.58	1.03	0.80	0.75	1.02
81	2.51	1.03	0.76	0.72	1.01
100	2.32	1.03	0.66	0.63	1.01
200	0.80	0.79	0.00	0.00	0.78
300	0.44	0.44	0.00	0.00	0.44
400	0.18	0.18	0.00	0.00	0.18
500	0.00	0.00	0.00	0.00	0.00

Table 4.2: Comparison between the non-Markovianity measures of $\mathcal{N}_{\text{PCA}} = \mathcal{N}_{\text{PC1}} + \mathcal{N}_{\text{PC2}} + \mathcal{N}_{\text{PC3}}$ and $\mathcal{N}_{\text{BLP}}$ for the same time interval. These values are related to the dynamical data illustrated in Figures 4.4, 4.5 and 4.8. The values of $\mathcal{N}_{\text{PC1}}$ and $\mathcal{N}_{\text{BLP}}$ are very similar to each other for $n_{\text{mean}} \geq 25$ (here highlighted in red).

For completeness, the calculation of $\mathcal{N}_{\text{BLP}}$ is also extended to the normalized time scale in terms of the revival time τ_r discussed in the previous sections. The results are presented analogously to the previous case in Table 4.3 and Figure 4.9. The results obtained are completely analogous to the discussion just carried out. It should be noted that there is also no direct relationship between $\mathcal{N}_{\text{BLP}}$ and n_{mean} on this normalized scale, as in the case of $\mathcal{N}_{\text{PCA}}$.

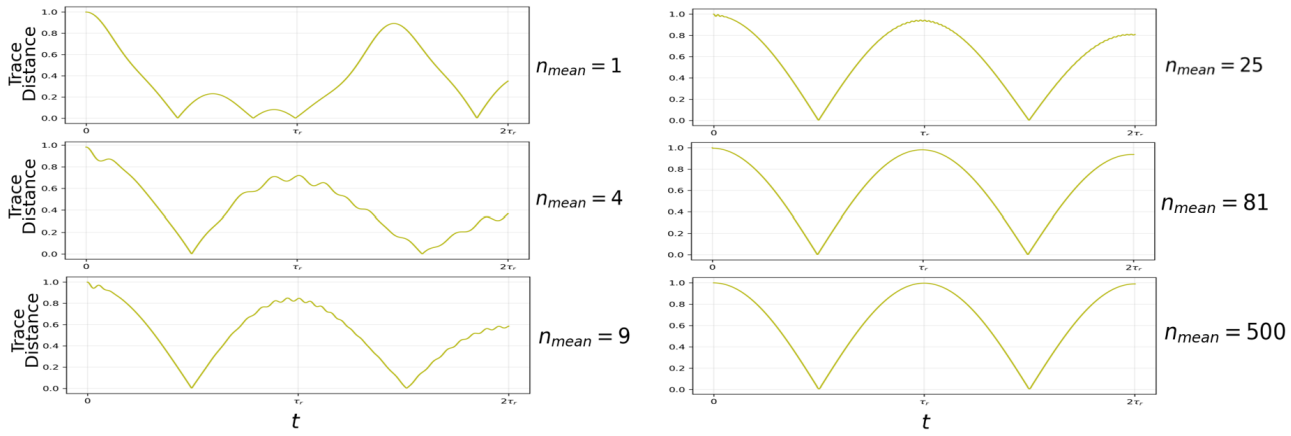

Figure 4.9: Time evolution of the trace distance between the proper pair of initial conditions that maximizes the non-Markovianity measure $\mathcal{N}_{\text{BLP}}$. Different values of the average number of photons n_{mean} present in the coherent radiation field were considered. An important remark is that a normalized time scale has been taken into account in terms of the revival time τ_r.

n_{mean}	$\mathcal{N}_{\text{PCA}}$ (Total)	$\mathcal{N}_{\text{PC1}}$	$\mathcal{N}_{\text{PC2}}$	$\mathcal{N}_{\text{PC3}}$	$\mathcal{N}_{\text{BLP}}$
1	4.88	1.33	1.83	1.71	2.85
4	4.21	1.44	1.46	1.31	4.12
9	5.19	1.51	1.84	1.84	3.81
16	5.66	1.70	2.00	1.96	3.59
25	5.20	1.80	1.74	1.66	1.76
36	5.58	1.90	1.89	1.80	1.84
49	5.55	1.94	1.85	1.76	1.88
64	5.30	1.96	1.72	1.62	1.91
81	5.01	1.97	1.57	1.47	1.91
100	4.67	1.97	1.40	1.31	1.93
200	3.86	1.96	0.96	0.95	1.96
300	3.87	1.97	0.95	0.94	1.97
400	3.90	1.98	0.97	0.95	1.98
500	3.88	1.98	0.95	0.95	1.97

Table 4.3: Comparison between the non-Markovianity measures of $\mathcal{N}_{\text{PCA}} = \mathcal{N}_{\text{PC1}} + \mathcal{N}_{\text{PC2}} + \mathcal{N}_{\text{PC3}}$ and $\mathcal{N}_{\text{BLP}}$ for a normalized time interval in terms of the revival time τ_r. These values are related to the dynamical data illustrated in Figures 4.6, 4.7 and 4.9. The values of $\mathcal{N}_{\text{PC1}}$ and $\mathcal{N}_{\text{BLP}}$ are very similar to each other for $n_{\text{mean}} \geq 25$ (here highlighted in red).

In what follows, a comparison is made between our method and some other methods present in the literature. It is noteworthy to clarify that the numerical values associated with the Figures and Tables above serve only as a reference, since the analysis made in this study has a more qualitative orientation. This is because no direct comparison was made between the results provided by our method and those provided by other methods. In part, the absence of this comparison resides in the first major advantage that our method offers over the others, since the computational efficiency is extremely superior. This is notoriously

more pronounced with respect to a substantial portion of the proposals in the literature that involve some kind of optimization, usually over all possible initial conditions. This is an advantage inherited from the PCA technique, which is very efficient for the treatment of high-dimensional data.

Now, the comparison will be made with the measure proposed by Rivas-Huelga-Plenio (RHP) [25], which is also frequently used in the literature, mainly for theoretical formulations. The comparison in this case is not so direct, since our measure is somewhat based on the distinguishability of quantum states, while RHP is based on the analysis of the dynamical maps themselves, and how much they deviate from the condition of being divisible. In the strict sense, someone could argue that RHP actually constitutes a measure of non-Markovianity, while our proposal (and many others based on information backflow processes) are only witnesses. This conflict was mentioned in the last part of Section 2.2.2, where it was said that the non-Markovianity measures based on the distinguishability of quantum states (like ours) imply the violation of the divisibility property of the dynamical map, but the converse is not necessarily true [41]. Whereas this is a matter of debate, we consider that a practical calculation of the degree of non-Markovianity of the system also plays an important role when thinking about possible applications of the system under study in answering the question whether the system is Markovian or not.

In this aspect, we consider that our proposal offers a great practical advantage as it is based on data analysis techniques. This means that for its correct implementation it is enough to know the possible states of the system at each instant of time, and not to know the dynamical maps themselves. The implementation in the Jaynes-Cummings model is not the best example of all, since its analytical solution is known, and from it (after an arduous effort) it is possible to know exactly the functional form of the mapping. However, in more complex models where it is necessary to use approximations in order to solve the dynamics, our method of data analysis is much more practical than the description of the dynamical map.

Finally, we would like to make a series of remarks regarding another method that may seem at first glance a little familiar to the one we are proposing. This is the proposal of studying the evolution of the volume in state space representation, also known as geometric characterization of non-Markovianity [53]. The similarities reside in the fact that the state space representation for a two dimensional system (like the JCM for example) is precisely the geometrical representation on the Bloch sphere. Therefore, studying the increases in the volume of the ellipsoids formed by the quantum states is the basis of that proposal. In fact, a connection with our idea could be found, since precisely the directions of maximum statistical variance of an ellipsoid are its semi-major axes. Hence, the PCA technique could also be implemented for the study of the the geometric measure.

However, the big difference between the two methods (apart from the process of formulation and numerical implementation) resides in the fact that they propose the study of changes in the volume, while we propose the study of changes in the PCs separately. Thus, if it is hypothetically the case that the PCs (which can also be seen as semi-major axes of the ellipsoid) change their lengths in such a way that the volume of the state space remains the same, our quanfier would detect a non-Markovian character as long as at least one of the PCs exhibits growth, while the geometrical proposal would detect nothing. As an example for the last sentence, the initial sphere collapses into a line segment where the volume is zero further on making the analysis from volume futile, where as our approaches keeps tracking non-Markovianity under those circumstances.

CHAPTER 5

Conclusions and Perspectives

The proposal presented in this work to quantify the non-Markovianity of a quantum system in an adequate way is based on the data analysis method known as principal component analysis (PCA), whereby the data, which in the present case represent the dynamics of the quantum states of an atom coupled to a coherent radiation field under the Jaynes-Cummings model (JCM), is decomposed into its most descriptive statistical factors. The non-Markovian quantifier $\mathcal{N}_{\text{PCA}}$ is defined as

$$\mathcal{N}_{\text{PCA}} = \sum_{i=1}^{3} \int_{\xi_i>0} \xi_i \, dt \, , \tag{5.1}$$

where the ξ_i are defined as

$$\xi_i = \frac{d}{dt} PC_{(i)} \, , \qquad i = 1, 2, 3 \, , \tag{5.2}$$

being the $PC_{(i)}$ lengths of the projections of the original data onto the directions of greatest statistical variance, here referred to as principal components (PCs). It is worth noting that it was found that the non-Markovian index $\mathcal{N}_{\text{PCA}}$ strongly depends on the time scale considered in the study.

The work was mostly focused on the dynamical study of pure states as atomic initial conditions. However, the analysis was extended to mixed initial states in Appendix A, where it was found that that by choosing mixed states instead of pure states, the index $\mathcal{N}_{\text{PCA}}$ is only rescaled by the radius of the initial sphere configuration, likewise the dynamical evolution of the PCs is also rescaled by the same factor. For the sake of simplicity, only initial configurations corresponding to spheres will be considered. However, the idea can be easily extrapolated to other initial configurations within the Bloch sphere.

This method was compared qualitatively with some of the most widely employed methods in the literature to measure the non-Markovianity of a system, among which are the Breuer-Laine-Piilo (BLP) measure based on the distinguishability of quantum states by trace distance [16], the Rivas-Huelga-Plenio (RHP) measure based directly on the non-divisibility of dynamical mappings [25], and the variation of the volume in the space of states [53]. We found advantages both from the point of view of the computational implementation and the interpretation of the results obtained. Therefore, we are confident in assuring that our non-Markovian quantifier based on the PCA technique constitutes a more suitable proposal to those currently used in this field of study. On the other side, a quantitative comparison has been carried out between the non-Markovianity indexes $\mathcal{N}_{\text{PCA}}$ and $\mathcal{N}_{\text{BLP}}$, where a similarity is observed between the calculated values of $\mathcal{N}_{\text{PC1}}$ (first principal component) and $\mathcal{N}_{\text{BLP}}$ for values of $n_{\text{mean}} \geq 25$. This gives an indication that the time evolution of the first principal component PC1 corresponds precisely to the time evolution of the trace distance between the proper initial atomic pair for $\mathcal{N}_{\text{PCA}}$.

For completeness of the discussion, in Appendix B the analysis of the temporal evolution of the state of the field (or environment) was performed. In particular, the environmental return fidelity, defined as the fidelity between the state of the field at an arbitrary time t with its initial state, was calculated. Nevertheless, no direct correlation was found between the environmental return fidelity and the non-Markovinaity index $\mathcal{N}_{\text{PCA}}$. Although fidelity also exhibits the phenomenon of revival, it is concluded that these quantities are not correlated with each other, at least not in an obvious way.

With reference now to the perspectives, the main one would be to apply the proposed methodology to other types of open quantum systems. The most direct case would be the generalizations of the Jaynes-Cummigs model, known as the Dicke model (without applying the RWA rotating wave approximation) [91] and the Traves-Cummings model (with RWA) [92,93]. The main difference with the JCM is that they consider more than one two-level atomic system. In this respect, these extensions can be used to model the coupling between two or more qubits, which is a topic of interest in the current development of quantum technologies.

In addition, there is also generalization of the representation in the Bloch sphere in a higher dimensional space N-level Bloch [94]. The ideas presented in this work can therefore be extended to other contexts. We must emphasize first that it is precisely in these high-dimensional spaces where the PCA technique is very useful to be employed; and second, that working with the Bloch sphere representation in two-level systems is friendly from the point of view of understanding and visualizing the dynamics of quantum states, but when considering physical systems with more degrees of freedom, it is no longer possible to represent pictorially what is happening. For two-level systems, the dynamics of the initial configuration of atomic states given by the Jaynes-Cummings model results in the formation of ellipsoids in the Bloch sphere representation, as observed during this work. This statement, however, cannot be extrapolated at this time to extensions of the JCM for more levels, as this is a topic beyond the scope of the present work. Nonetheless, since the PCA is applied directly to a data set (which in this case corresponds to the time evolution of quantum states), we are confident that regardless of the shape of the points in the space of the atomic density matrices at later times, the non-Markovianity index $\mathcal{N}_{\text{PCA}}$ is still an appropriate measure, given that the initial configuration is known.

In this regard, although the two-level model may seem like an extreme idealization, it is very useful for understanding the use of the concepts and tools presented during this work. Once understood, for example, the physical information contained in the principal components and the interpretation that can be given to their changes over time, it is easier to extrapolate the technique to more complex systems and to understand correctly what is happening.

APPENDIX A

Mixed States Analysis

As already seen in Section 3.3, the reduced density matrix for the atomic system can be calculated from the three cartesian components of the Bloch vector $\mathbf{r}(t) = (\, u(t), v(t), w(t)\,)$. This relation is given by

$$\rho_{\text{atom}}(t) = \begin{bmatrix} \rho_{gg}(t) & \rho_{ge}(t) \\ \rho_{eg}(t) & \rho_{ee}(t) \end{bmatrix} = \frac{1}{2} \begin{bmatrix} 1 + w(t) & u(t) - iv(t) \\ u(t) + iv(t) & 1 - w(t) \end{bmatrix}. \tag{A.1}$$

It has also been mentioned that the points just on the surface of the Bloch sphere correspond to the pure states of the atom (i.e. coherent superposition of the $|g\rangle$, $|e\rangle$ states), while its interior points correspond to the set of mixed states. The time evolution of the quantum states is regarded as a situation easy to deal with, given that the initial state is precisely a pure state. This is because the expression for the dynamical evolution of the state of the composed system is well-known and simple (see equations 3.32 and 3.33). However, it may also be interesting to study the dynamics of the system when the initial state of the atom is a mixed state.

The strategy suggested is to determine the density matrix of the atom at the initial instant ($t = 0$) from the initial distribution of points in the Bloch sphere representation. In spherical coordinates, the three Cartesian components are parameterized by

$$\begin{aligned} u(t=0) &= r\cos\varphi\sin\theta\,, \\ v(t=0) &= r\sin\varphi\sin\theta\,, \\ w(t=0) &= r\cos\theta\,. \end{aligned} \tag{A.2}$$

In particular, $r = 1$ represents the situation where all points are on the surface of the Bloch sphere, whereas $r < 1$ represents an initial sphere configuration completely within the Bloch sphere (see the configuration at $t = 0$ of the Figure A.1 for $r \approx 0.63$). It is important to clarify that in the following analysis, for the sake of simplicity, only initial configurations corresponding to spheres will be considered. However, the idea can be easily extrapolated to other initial configurations within the Bloch sphere.

For the calculation of the dynamics of the composed system (whose initial state is $\chi(0) = \rho_{\text{atom}}(0) \otimes \rho_{\text{field}}(0)$), the Python library QuTiP will be used, which is oriented to the simulation of quantum systems, particularly open quantum systems. It is worth highlighting that, for our current task of simulating the dynamics of all the points that make up the initial configuration, the use of this library naturally results in a higher computational cost than the procedures already implemented throughout this work. Nevertheless, this is the price to pay to avoid the analytical calculation of the dynamics, which can be somewhat cumbersome in the present case.

Below, a fragment of the code implemented to calculate the time evolution of the atomic reduced density matrix is presented.

```
import numpy as np
import qutip as qtp

# ... (definition of parameters)

#convert the matrix into a qutip object
rho_atom_init = qtp.Qobj( np.array([[pee_0[i], peg_0[i]], [pge_0[i], pgg_0[i]]]) )
#density matrix (dm) for a coherent state
rho_field_init = qtp.coherent_dm( n_final + 1, np.sqrt(n_mean) )
rho_total_init = qtp.tensor( rho_atom_init, rho_field_init )

a = qtp.tensor( qtp.qeye(2), qtp.destroy(n_final + 1) )   #bosonic annihilation operator
sigma_minus = qtp.tensor( qtp.sigmam(), qtp.qeye(n_final + 1) )
H = g * ( a * sigma_minus.dag() + a.dag() * sigma_minus )   #interaction Hamiltonian
#QuTiP tool for solving the dynamics given the Hamiltonian, initial state and time
result = qtp.mesolve(H, rho_total_init, t, [], [])

time = 10   #time index
reduced_rho_atom = result.states[time].ptrace(0)    #"ptrace": partial trace operation
```

Once the atomic reduced density matrix is known in the defined time interval, equation A.1 can be used again to plot the dynamics on the Bloch sphere, as has been done throughout this work. For the particular case of an initial state of coherent light with $n_{\text{mean}} = 9$ and a radius of $r \approx 0.63$ in the initial atomic configuration, the dynamics is illustrated in Figure A.1.

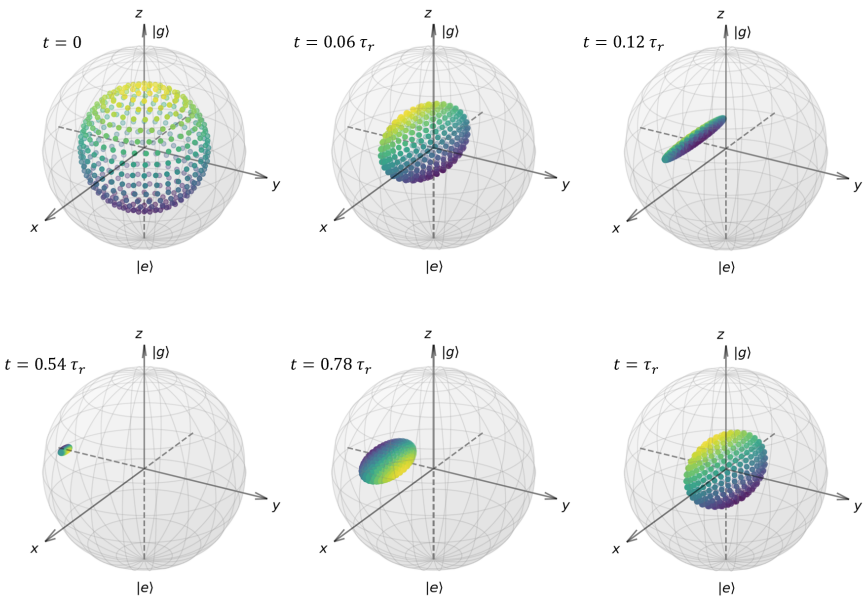

Figure A.1: Evolution of the sphere of initial mixed states of the atom when it is coupled to a radiation field described by a coherent state of light with mean number of photons equal to $n_{\text{mean}} = 9$. The radius of the initial sphere was chosen to be $r \approx 0.63$. It is convenient to compare it with Figure 3.9 to see the similarities between the dynamics of pure and mixed states.

The choice of these parameters was not random, but was made for the purpose of making a direct comparison with the dynamics of the initial configuration of pure states interacting with the same initial field state, which is illustrated in Figure 3.9. It is evident that the dynamics are practically the same in both cases,

differing only by the scale factor given by the radius of the mixed state sphere.

Now, before applying PCA to the generated dataset, one consideration must be reviewed. According to the Section 4.2, it is necessary to scale the lengths of the principal components PCs (projections of the data along the directions of maximal variance) by some factor to fairly match the original data rather than the standardized data, in order to fulfill our concrete purpose of correctly interpreting the PCs on a physical ground. In the present case, the scale factor must be defined in terms of the radius of the initial sphere, in a similar way to what was already explained in the aforementioned section

```
scale = radius / length[0,0]   # or length[0,1], or length[0,2] since it is a sphere
```

For pure states, it is clear that the scale factor of Section 4.2 is recovered, since the initial sphere radius is equal to 1.

In this order of ideas, the time evolution of the PCs is determined and depicted in Figure A.2 for different purity P values, which are given by [28]

$$P = \frac{1}{2}\left(\,|\mathbf{r}|^2 + 1\,\right), \quad \text{where} \quad \frac{1}{2} \leq P \leq 1\,, \tag{A.3}$$

being $\mathbf{r}$ is the Bloch vector. The purity P gives information on how much a state is mixed.

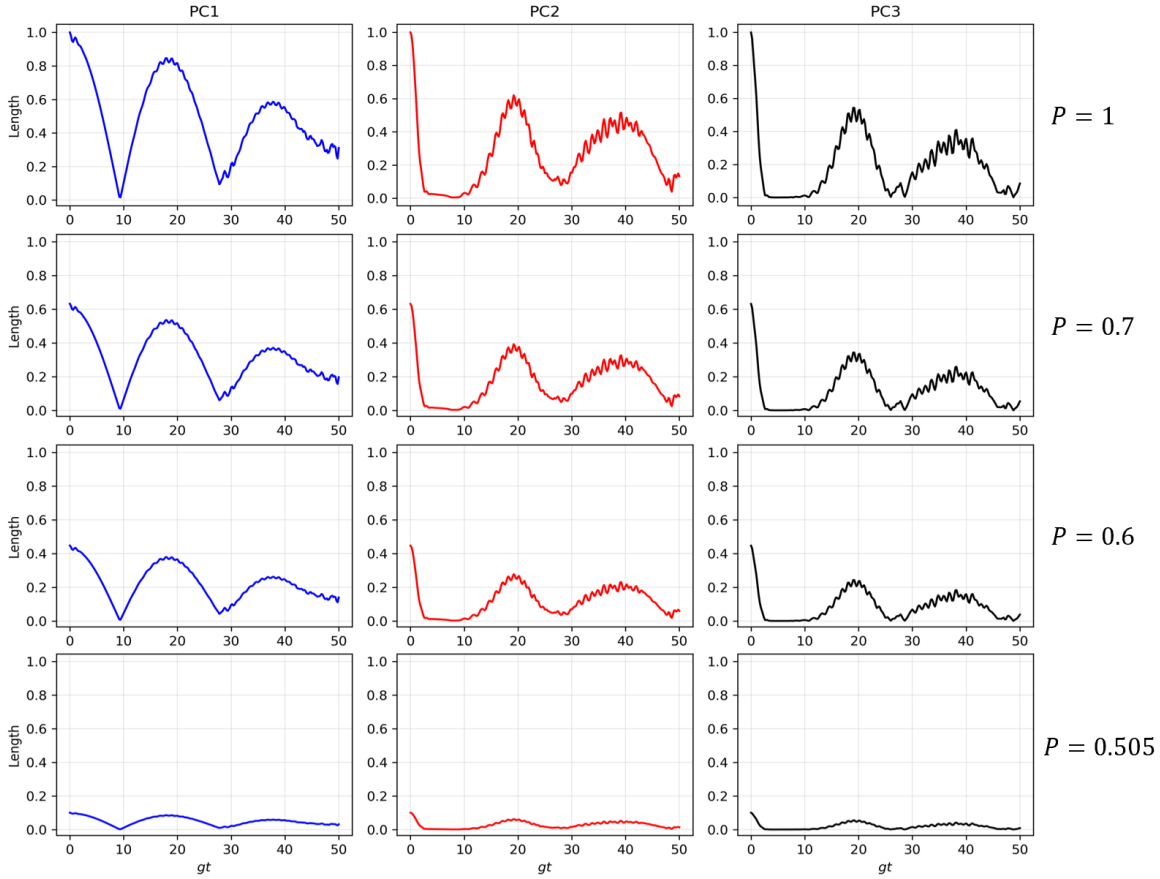

Figure A.2: Time evolution of the three principal components PCs for different values of the purity P. The initial field state is a coherent state with $n_{\text{mean}} = 9$. It is clear that the PCs are only rescaled by a factor that depends on the purity value (or equivalently on the sphere radius).

Finally, the direct proportionality between the non-Markovianity index $\mathcal{N}_{\text{PCA}}$ and the radius of the initial sphere becomes evident when observing Figure A.3, where the value of $\mathcal{N}_{\text{PCA}}$ is plotted as a function of the radius (left) and the purity (right).

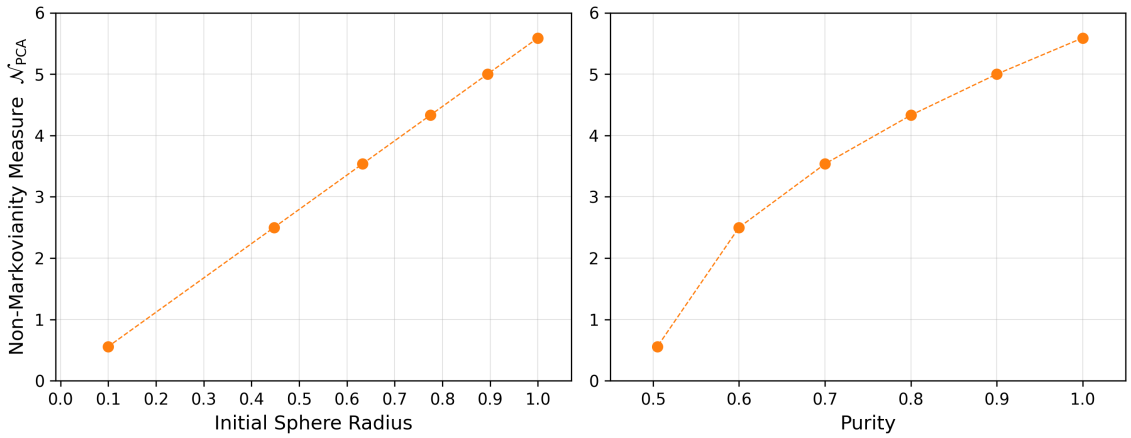

Figure A.3: Non-Markovianity index $\mathcal{N}_{\text{PCA}}$ as a function of the radius of the initial configuration of mixed states (left) and of the purity (right). The proporcionality between $\mathcal{N}_{\text{PCA}}$ and the radius is evident.

It is then concluded that the dynamics of mixed states is analogous to that of pure states, being a scale factor equal to the radius of the initial sphere of atomic states what makes the difference between them.

APPENDIX B

Environmental Return Fidelity

The composed quantum system discussed along this work consists of two quantum subsystems: the atom and the radiation field. So far, we have focused our attention and analysis exclusively on the dynamical behavior of the two-level atomic system (who has been referred to as the open quantum system of interest). In contrast, a study of the time evolution of the environmental state encompasses a topic of interest by its own, or could help to complement the analysis of the non-Markovian behavior of an open quantum system [95]. In this Appendix, our study will be more concerned with the second aspect, where we will look for a relationship between the time evolution of the field state with the non-Markovianity index $\mathcal{N}_{\text{PCA}}$.

The reduced density matrix of the field $\rho_E(t)$ can be obtained from the density matrix of the composed system $\chi(t)$ by tracing over the atomic degrees of freedom. For the simple case of a two-level atomic system (whose Hilbert space is spanned by the states $|e\rangle$ and $|g\rangle$), this is very straightforward since only two terms need to be considered. So, the reduced density matrix of the field is given by

$$\rho_E(t) = \langle e|\, \chi(t)\, |e\rangle \;+\; \langle g|\, \chi(t)\, |g\rangle \;. \tag{B.1}$$

Evoking equation 3.32 (for initial pure atomic states), the above expression expands as

$$\begin{aligned} \rho_E(t) \;\; &= \;\; |c_{e,0}(t)|^2\, |0\rangle\langle 0| \;+\; \sum_{n=1} \left[\, c^*_{e,n}(t)\, c_{e,0}(t)\, |n\rangle\langle 0| \;+\; c.c.\, \right] \\ &+ \;\; \sum_{nm=1} \left[\, c_{e,n}(t)\, c^*_{e,m}(t) \;+\; c_{g,n}(t)\, c^*_{g,m}(t)\, \right] \, |n\rangle\langle m| \;, \end{aligned} \tag{B.2}$$

where $c.c$ stands for complex conjugate. The coefficients of the expanssion are given by equation 3.34 for the resonant case.

Knowing then the state of the field for an arbitrary time t, one way to quantify the similarity between it and its initial state is through the physical quantity known as fidelity, which takes as arguments two density matrices and is defined by [28]

$$F(\rho,\sigma) = \left(\text{tr}\sqrt{\sqrt{\rho}\sigma\sqrt{\rho}}\right)^2 \;. \tag{B.3}$$

The values of $F(\rho,\sigma)$ are bounded to the interval $[0,1]$, being $F(\rho,\sigma)=1$ if and only if $\rho=\sigma$.

Here we will adopt the term "*Environmental Return Fidelity*" to refer to the fidelity between the state of the field at an arbitrary time t and its initial state. The calculation of fidelity will be done with the help of QuTiP library of Python, already introduced in Appendix A. However, the dynamics of $\rho_E(t)$ is calculated using the equation B.2. Below, a fragment of the code is shown.

```
import numpy as np
import qutip as qtp

# ... (definition of parameters)

#density matrix (dm) for a coherent state
rho_field_init = qtp.coherent_dm( n_final + 1, np.sqrt(n_mean) )

# ... ( calculation of rho_E for each time as an np.array([]) )

reduced_rho_field = qtp.Qobj(matrix)  #convert the matrix to a qutip object
fidelity = qtp.metrics.fidelity(rho_field_init, reduced_rho_field)
```

When making a direct comparison between the non-Markovianity index $\mathcal{N}_{\text{PCA}}$ and the environmental return fidelity, one faces a problem. On the one hand, the fidelity compares two density matrices, while $\mathcal{N}_{\text{PCA}}$ is a joint quantity that depends on all the points that make up the configuration in the space of the density matrices of the atom (whose visualization is carried out using the Bloch sphere representation). Since, for a given time, the return fidelity takes a different value for each initial atomic state considered, this implies that the return fidelity must also be defined as a joint quantity for the sake of consistency. Thus, a first proposal could be to calculate the arithmetic mean over all possible initial states of the atom in each snapshot as a definition of the environmental return fidelity. This idea is depicted in Figure B.1a.

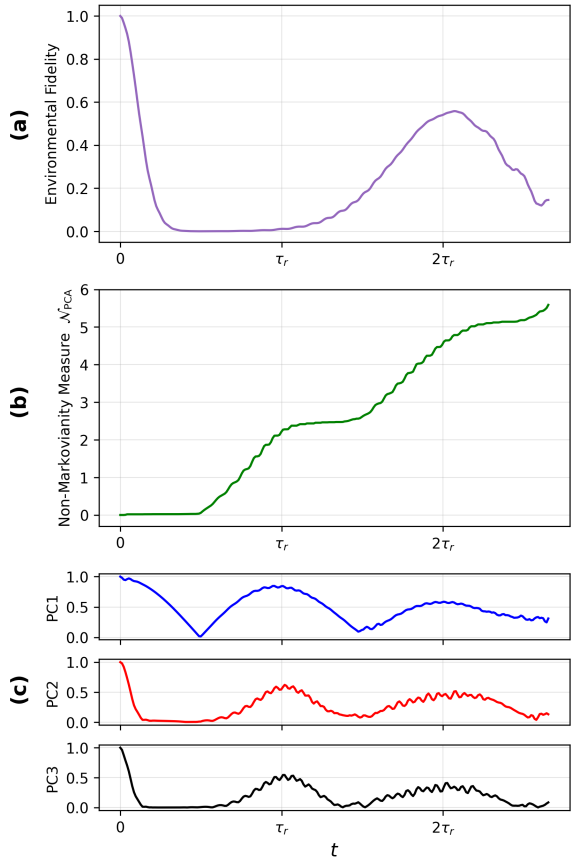

Figure B.1: Comparison between the dynamical behavior of **(a)** the mean-defined environmental return fidelity, **(b)** the non-Markovianity index $\mathcal{N}_{\text{PCA}}$, and **(c)** the three principal components PCs. The initial field state is a coherent state with average photon number $n_{\text{mean}} = 9$ and τ_r is its associated revival time.

The Subfigures B.1b and B.1c were included to provide a direct comparison between the dynamics of the $\mathcal{N}_{\text{PCA}}$ index and the three principal components PCs with the value of environmental return fidelity. When comparing, there is no clear relationship between the dynamics of the quantities illustrated in the Subfigure B.1a with the Subfigures B.1b and B.1c. Although fidelity also exhibits the phenomenon of revival, it is concluded that these quantities are not correlated with each other, at least not in an obvious way.

The lack of correlation in the quantities could be attributed to the definition of environmental return fidelity given here. Other options could be to define the environmental return fidelity as the maximum or minimum value at each time snapshot instead of the arithmetic mean (see Figure B.2 (left)), or to follow a similar line of thought as in the definition of the $\mathcal{N}_{\text{PCA}}$ or the $\mathcal{N}_{\text{BLP}}$ indexes, and define it as the value given by the initial atomic state that maximize the integral of the positive or negative derivatives of the fidelity (see Figure B.2 (right)). However, the dynamics of each case are very similar to the original proposal based on the arithmetic mean, so the stated conclusion remains.

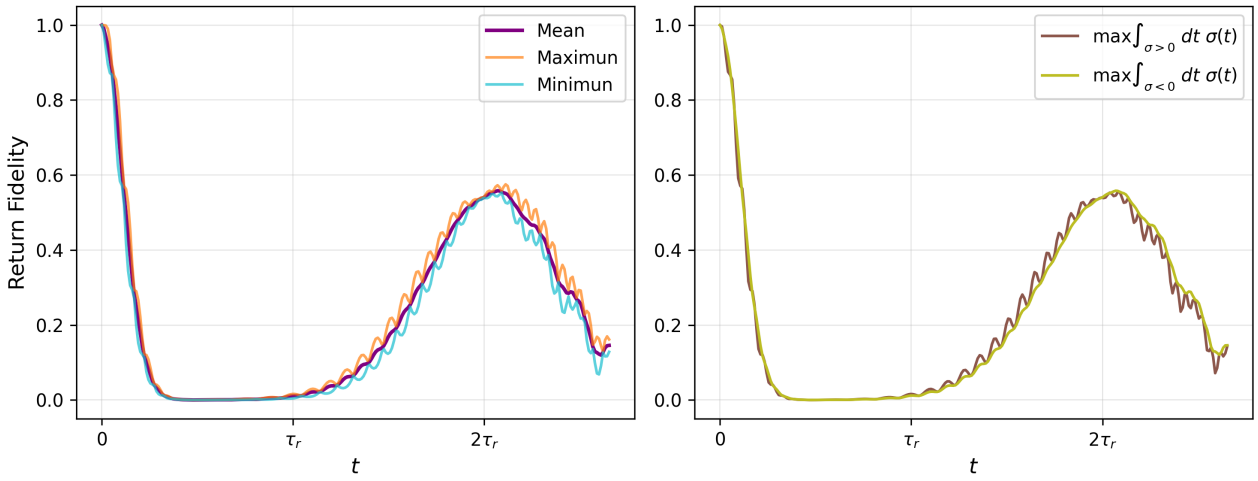

Figure B.2: Temporal evolution of the different proposals to define the environmental return fidelity as a joint measure of the initial atomic states for each temporal snapshot. On the left, the main proposal based on the arithmetic mean is shown together with two proposals based on the maximum and minimum value of the fidelity at each instant. On the right, two proposals influenced by the definition of the non-Markovianity index $\mathcal{N}_{\text{BLP}}$ are shown, where the initial atomic state that maximizes the integral of the positive or negative derivatives of the fidelity is considered. Nonetheless, all cases have very similar behavior to each other.

Bibliography

[1] W. Nolting, *Theoretical Physics 6: Quantum Mechanics - Basics*, Springer Cham, 1 ed., 2017.

[2] M. Schlosshauer, *Decoherence and the Quantum-To-Classical Transition*, Springer Berlin, Heidelberg, 1 ed., 2007.

[3] H.-P. Breuer and F. Petruccione, *The theory of open quantum systems*, Oxford University Press, 1 ed., 2002.

[4] A. Rivas and S. F. Huelga, *Open Quantum Systems: An Introduction*, Springer Berlin, Heidelberg, 1 ed., 2012.

[5] M. Merkli, *Quantum markovian master equations: Resonance theory shows validity for all time scales*, Annals of Physics, 412 (2020), p. 167996.

[6] G. Lindblad, *On the generators of quantum dynamical semigroups*, Commun.Math. Phys., 48 (1976), pp. 119–130.

[7] V. Gorini, A. Kossakowski, and E. C. G. Sudarshan, *Completely positive dynamical semigroups of N-level systems*, Journal of Mathematical Physics, 17 (1976), pp. 821–825.

[8] B. Liu and et al., *Experimental control of the transition from Markovian to non-Markovian dynamics of open quantum systems*, Nature Phys., 7 (2011), pp. 931–934.

[9] N. Bernardes and et al., *Experimental observation of weak non-Markovianity*, Sci Rep, 5 (2015), p. 17520.

[10] K. Wu and et al., *Detecting non-Markovianity via quantified coherence: theory and experiments*, npj Quantum Inf, 6 (2020), p. 55.

[11] J. Sun, Y.-N. Sun, C. feng Li, G.-C. Guo, K. Luoma, and J. Piilo, *Non-markovian discrete qubit dynamics*, Science Bulletin, 61 (2016), pp. 1031–1036.

[12] J. F. Haase, P. J. Vetter, T. Unden, A. Smirne, J. Rosskopf, B. Naydenov, A. Stacey, F. Jelezko, M. B. Plenio, and S. F. Huelga, *Controllable non-markovianity for a spin qubit in diamond*, Phys. Rev. Lett., 121 (2018), p. 060401.

[13] B.-W. Li, Q.-X. Mei, Y.-K. Wu, M.-L. Cai, Y. Wang, L. Yao, Z.-C. Zhou, and L.-M. Duan, *Observation of non-markovian spin dynamics in a jaynes-cummings-hubbard model using a trapped-ion quantum simulator*, Phys. Rev. Lett., 129 (2022), p. 140501.

[14] Y. Dong and et al, *Non-Markovianity-assisted high-fidelity Deutsch–Jozsa algorithm in diamond*, npj Quantum Inf, 4 (2018), p. 3.

[15] F. WANG, P.-Y. HOU, Y.-Y. HUANG, W.-G. ZHANG, X.-L. OUYANG, X. WANG, X.-Z. HUANG, H.-L. ZHANG, L. HE, X.-Y. CHANG, AND L.-M. DUAN, *Observation of entanglement sudden death and rebirth by controlling a solid-state spin bath*, Phys. Rev. B, 98 (2018), p. 064306.

[16] H.-P. BREUER, E.-M. LAINE, AND J. PIILO, *Measure for the degree of non-markovian behavior of quantum processes in open systems*, Phys. Rev. Lett., 103 (2009), p. 210401.

[17] S. HASELI AND ET AL., *Non-markovianity through flow of information between a system and an environment*, Phys. Rev. A, 90 (2014), p. 052118.

[18] S. DEFFNER AND E. LUTZ, *Quantum speed limit for non-markovian dynamics*, Phys. Rev. Lett., 111 (2013), p. 010402.

[19] D. REICH, N. KATZ, AND C. KOCH, *Exploiting Non-Markovianity for Quantum Control*, Sci Rep, 5 (2015), p. 12430.

[20] E. LAINE, H.-P. BREUER, AND J. PIILO, *Nonlocal memory effects allow perfect teleportation with mixed states*, Sci Rep, 4 (2014), p. 4620.

[21] B. BYLICKA, D. CHRUŚCIŃSKI, AND S. MANISCALCO, *Non-Markovianity and reservoir memory of quantum channels: a quantum information theory perspective*, Sci Rep, 4 (2014), p. 5720.

[22] G.-Y. XIANG, Z.-B. HOU, C.-F. LI, G.-C. GUO, H.-P. BREUER, E.-M. LAINE, AND J. PIILO, *Entanglement distribution in optical fibers assisted by nonlocal memory effects*, Europhysics Letters, 107 (2014), p. 54006.

[23] A. ALTHERR AND Y. YANG, *Quantum metrology for non-markovian processes*, Phys. Rev. Lett., 127 (2021), p. 060501.

[24] G. THOMAS, N. SIDDHARTH, S. BANERJEE, AND S. GHOSH, *Thermodynamics of non-markovian reservoirs and heat engines*, Phys. Rev. E, 97 (2018), p. 062108.

[25] A. RIVAS, S. F. HUELGA, AND M. B. PLENIO, *Entanglement and non-markovianity of quantum evolutions*, Phys. Rev. Lett., 105 (2010), p. 050403.

[26] H. GOLDSTEIN, *Classical Mechanics*, Addison Wesley, Boston, 3 ed., 2002.

[27] H. J. CARMICHAEL, *Statistical Methods of Quantum Optics I: Master Equations and Fokker-Planck Equations*, Springer Berlin, Heidelberg, 1 ed., 1999.

[28] M. A. NIELSEN AND I. L. CHUANG, *Quantum Computation and Quantum Information: 10th Anniversary Edition*, Cambridge University Press, 2010.

[29] G. A. PAVLIOTIS, *Markov processes and the chapman–kolmogorov equation*, in Stochastic Processes and Applications, Springer New York, NY, 1 ed., 2024, pp. 30–34.

[30] A. A. BUDINI, *Lindblad rate equations*, Phys. Rev. A, 74 (2006), p. 053815.

[31] S. CHATURVEDI AND F. SHIBATA, *Time-convolutionless projection operator formalism for elemination of fast variables*, Z Physik B, 35 (1979), pp. 297–308.

[32] R. FEYNMAN AND F. VERNON, *The theory of a general quantum system interacting with a linear dissipative system*, Annals of Physics, 24 (1963), pp. 118–173.

[33] A. CALDEIRA AND A. LEGGETT, *Path integral approach to quantum brownian motion*, Physica A: Statistical Mechanics and its Applications, 121 (1983), pp. 587–616.

[34] C. GARDINER AND P. ZOLLER, *Quantum Noise: A Handbook of Markovian and Non-Markovian Quantum Stochastics Methods with Applications to Quantum Optics*, Addison Wesley, Boston, 3 ed., 2004.

[35] K. KRAUS, A. BÖHM, J. DOLLARD, AND W. WOOTERS, *States, Effects, and Operations: Fundamental Notions of Quantum Theory*, Springer Berlin, Heidelberg, 1 ed., 1983.

[36] A. JAMIOŁKOWSKI, *Linear transformations which preserve trace and positive semidefiniteness of operators*, Reports on Mathematical Physics, 3 (1972), pp. 275–278.

[37] M.-D. CHOI, *Completely positive linear maps on complex matrices*, Linear Algebra and its Applications, 10 (1975), pp. 285–290.

[38] M. MALEK-SHAHMIRZADI, *A characterization of certain classes of matrix norms*, Linear and Multilinear Algebra, 13 (1983), pp. 97–99.

[39] C. ADDIS, B. BYLICKA, D. CHRUŚCIŃSKI, AND S. MANISCALCO, *Comparative study of non-markovianity measures in exactly solvable one- and two-qubit models*, Phys. Rev. A, 90 (2014), p. 052103.

[40] S. WISSMANN, A. KARLSSON, E.-M. LAINE, J. PIILO, AND H.-P. BREUER, *Optimal state pairs for non-markovian quantum dynamics*, Phys. Rev. A, 86 (2012), p. 062108.

[41] D. CHRUŚCIŃSKI, A. KOSSAKOWSKI, AND A. RIVAS, *Measures of non-markovianity: Divisibility versus backflow of information*, Phys. Rev. A, 83 (2011), p. 052128.

[42] D. BURES, *An extension of kakutani's theorem on infinite product measures to the tensor product of semifinite w*-algebras*, Trans. Amer. Math. Soc., 135 (1969), pp. 199–212.

[43] S.-X. WU AND C.-S. YU, *Quantum speed limit based on the bound of bures angle*, Scientific Reports, 10 (2020), p. 5500.

[44] S. L. BRAUNSTEIN AND C. M. CAVES, *Statistical distance and the geometry of quantum states*, Phys. Rev. Lett., 72 (1994), pp. 3439–3443.

[45] Z. HE, H.-S. ZENG, Y. LI, Q. WANG, AND C. YAO, *Non-markovianity measure based on the relative entropy of coherence in an extended space*, Phys. Rev. A, 96 (2017), p. 022106.

[46] S. M. HOSSEINY, J. SEYED-YAZDI, AND M. NOROUZI, *Witness of non-markovian dynamics based on bhattacharyya quantum distance*, Scientific Reports, 14 (2024), p. 18261.

[47] D. PETZ, *Monotone metrics on matrix spaces*, Linear Algebra and its Applications, 244 (1996), pp. 81–96.

[48] S. LUO, S. FU, AND H. SONG, *Quantifying non-markovianity via correlations*, Phys. Rev. A, 86 (2012), p. 044101.

[49] X.-M. LU, X. WANG, AND C. P. SUN, *Quantum fisher information flow and non-markovian processes of open systems*, Phys. Rev. A, 82 (2010), p. 042103.

[50] M. J. W. HALL, J. D. CRESSER, L. LI, AND E. ANDERSSON, *Canonical form of master equations and characterization of non-markovianity*, Phys. Rev. A, 89 (2014), p. 042120.

[51] Z. HE, C. YAO, Q. WANG, AND J. ZOU, *Measuring non-markovianity based on local quantum uncertainty*, Phys. Rev. A, 90 (2014), p. 042101.

[52] F. F. FANCHINI, G. KARPAT, B. ÇAKMAK, L. K. CASTELANO, G. H. AGUILAR, O. J. FARÍAS, S. P. WALBORN, P. H. S. RIBEIRO, AND M. C. DE OLIVEIRA, *Non-markovianity through accessible information*, Phys. Rev. Lett., 112 (2014), p. 210402.

[53] S. Lorenzo, F. Plastina, and M. Paternostro, *Geometrical characterization of non-markovianity*, Phys. Rev. A, 88 (2013), p. 020102.

[54] F. F. Fanchini, G. b. u. Karpat, D. Z. Rossatto, A. Norambuena, and R. Coto, *Estimating the degree of non-markovianity using machine learning*, Phys. Rev. A, 103 (2021), p. 022425.

[55] A. R. Morgillo, M. F. Sacchi, and C. Macchiavello, *Detecting markovianity of quantum processes via recurrent neural networks*, arXiv preprint arXiv:2406.07226, (2024).

[56] E. Jaynes and F. Cummings, *Comparison of quantum and semiclassical radiation theories with application to the beam maser*, Proceedings of the IEEE, 51 (1963), pp. 89–109.

[57] D. B. Tretyakov, V. M. Entin, E. A. Yakshina, I. I. Beterov, C. Andreeva, and I. I. Ryabtsev, *Controlling the interactions of a few cold rb rydberg atoms by radio-frequency-assisted förster resonances*, Phys. Rev. A, 90 (2014), p. 041403.

[58] Y. Tabuchi, S. Ishino, A. Noguchi, T. Ishikawa, R. Yamazaki, K. Usami, and Y. Nakamura, *Coherent coupling between a ferromagnetic magnon and a superconducting qubit*, Science, 349 (2015), pp. 405–408.

[59] D. Lachance-Quirion, Y. Tabuchi, S. Ishino, A. Noguchi, T. Ishikawa, R. Yamazaki, and Y. Nakamura, *Resolving quanta of collective spin excitations in a millimeter-sized ferromagnet*, Science Advances, 3 (2017), p. e1603150.

[60] I. I. Rabi, *Space quantization in a gyrating magnetic field*, Phys. Rev., 51 (1937), pp. 652–654.

[61] K. A. Tomilin, *Natural Systems of Units. To the Centenary Anniversary of the Planck System*, in 21st International Workshop on the Fundamental Problems of High-Energy Physics and Field Theory, 1998, pp. 287–296.

[62] F. Schwabl, *Motion in an electromagnetic field*, in Quantum Mechanics, Springer Berlin, Heidelberg, 4 ed., 2007, ch. 7, pp. 143–157.

[63] D. J. Griffiths, *Introduction to Electrodynamics*, Cambridge University Press, 4 ed., 2017.

[64] C. Cohen-Tannoudji, *Quantum electrodynamics in the coulomb gauge*, in Photons and Atoms, John Wiley & Sons, Ltd, 1997, ch. 3, pp. 169–252.

[65] C. Gerry and P. Knight, *Introductory Quantum Optics*, Cambridge University Press, 2004.

[66] D. W. Sciama, *The physical significance of the vacuum state of a quantum field*, in Saunders, S. and Brown, H.R., Eds., The Philosophy of Vacuum, Oxford University Press, 1991, pp. 137–158.

[67] S. Weinberg, *The Quantum Theory of Fields*, Cambridge University Press, 1 ed., 1995.

[68] B. Zwiebach, *Mastering Quantum Mechanics: Essentials, Theory, and Applications*, The MIT Press, 1 ed., 2022.

[69] J. Larson and T. Mavrogordatos, *The Jaynes–Cummings Model and Its Descendants*, 2053-2563, IOP Publishing, 2021.

[70] G. S. Agarwal, *Rotating-wave approximation and spontaneous emission*, Phys. Rev. A, 7 (1973), pp. 1195–1197.

[71] M. O. Scully and M. S. Zubairy, *Quantum Optics*, Cambridge University Press, 1 ed., 1997.

[72] R. Omnès, *The Interpretation of Quantum Mechanics*, Princeton University Press, 1 ed., 1994.

[73] Y. HIROYUKI AND K. UJIHARA, *Spontaneous Emission and Laser Oscillation in Microcavities*, CRC Press, 1 ed., 1995.

[74] D. WALLS AND G. J. MILBURN, *Quantum Optics*, Springer Berlin, Heidelberg, 2 ed., 2008.

[75] S. M. ROSS, *Introduction to Probability Models*, Academic Press, 11 ed., 2014.

[76] F. BLOCH, *Nuclear induction*, Phys. Rev., 70 (1946), pp. 460–474.

[77] J. GEA-BANACLOCHE, *A new look at the jaynes-cummings model for large fields: Bloch sphere evolution and detuning effects*, Optics Communications, 88 (1992), pp. 531–550.

[78] J. GEA-BANACLOCHE, *Collapse and revival of the state vector in the jaynes-cummings model: An example of state preparation by a quantum apparatus*, Phys. Rev. Lett., 65 (1990), pp. 3385–3388.

[79] J. E. ELSE SALLY RUANE AND H. SOUTHALL, *Data in Society: Challenging Statistics in an Age of Globalisation*, Briston University Press, 2019.

[80] C. KIM, K. D. PARK, AND J.-K. RHEE, *Quantum error mitigation with artificial neural network*, IEEE Access, 8 (2020), pp. 188853–188860.

[81] D. KOUTNÝ, L. GINÉS, M. MOCZAŁA-DUSANOWSKA, S. HÖFLING, C. SCHNEIDER, A. PREDOJEVIĆ, AND M. JEŽEK, *Deep learning of quantum entanglement from incomplete measurements*, Science Advances, 9 (2023), p. eadd7131.

[82] C. HARNEY, M. PATERNOSTRO, AND S. PIRANDOLA, *Mixed state entanglement classification using artificial neural networks*, New Journal of Physics, 23 (2021), p. 063033.

[83] I. KHAIT, J. CARRASQUILLA, AND D. SEGAL, *Optimal control of quantum thermal machines using machine learning*, Phys. Rev. Res., 4 (2022), p. L012029.

[84] P. P. MAZZA, D. ZIETLOW, F. CAROLLO, S. ANDERGASSEN, G. MARTIUS, AND I. LESANOVSKY, *Machine learning time-local generators of open quantum dynamics*, Phys. Rev. Res., 3 (2021), p. 023084.

[85] S. SGROI, G. M. PALMA, AND M. PATERNOSTRO, *Reinforcement learning approach to nonequilibrium quantum thermodynamics*, Phys. Rev. Lett., 126 (2021), p. 020601.

[86] L. BANCHI, E. GRANT, A. ROCCHETTO, AND S. SEVERINI, *Modelling non-markovian quantum processes with recurrent neural networks*, New Journal of Physics, 20 (2018), p. 123030.

[87] S. L. BRUNTON AND J. N. KUTZ, *Data-Driven Science and Engineering: Machine Learning, Dynamical Systems, and Control*, Cambridge University Press, 2019.

[88] J. BISGARD, *Analysis and Linear Algebra: The Singular Value Decomposition and Applications*, Student Mathematical Library. AMS, 1 ed., 2021.

[89] G. R. NAIK, *Advances in Principal Component Analysis*, Springer Singapore, 1 ed., 2018.

[90] I. T. JOLLIFFE AND J. CADIMA, *Principal component analysis: a review and recent developments*, Trans. R. Soc. A., 374 (2016), p. 20150202.

[91] R. H. DICKE, *Coherence in spontaneous radiation processes*, Phys. Rev., 93 (1954), pp. 99–110.

[92] M. TAVIS AND F. W. CUMMINGS, *Exact solution for an n-molecule—radiation-field hamiltonian*, Phys. Rev., 170 (1968), pp. 379–384.

[93] Y.-T. CHUANG, M.-W. LEE, AND L.-Y. HSU, *Tavis-cummings model revisited: A perspective from macroscopic quantum electrodynamics*, Frontiers in Physics, 10 (2022).

[94] G. KIMURA, *The bloch vector for n-level systems*, Physics Letters A, 314 (2003), pp. 339–349.

[95] D. GRIBBEN, A. STRATHEARN, G. E. FUX, P. KIRTON, AND B. W. LOVETT, *Using the Environment to Understand non-Markovian Open Quantum Systems*, Quantum, 6 (2022), p. 847.